Heat Transfer and Friction Factor Characteristics of Double Pass Solar Air Heater Having W-Shaped Artificial Roughness on Absorber plate

DISSERTATION

Submitted in partial fulfillment of the

Requirement for the award of the Degree of

MASTER OF TECHNOLOGY

In

MECHANICAL ENGINEERING

By

MANISH KUMAR TATED

(11004227)

Under the Guidance of

Mr. SUNDHASHU DOGRA

DEPARTMENT OF MECHANICAL ENGINEERING

LOVELY PROFESSIONAL UNIVERSITY

PHAGWARA, PUNJAB (INDIA)-144402

2015

Lovely Professional University Jalandhar, Punjab

CERTIFICATE

I hereby certify that the work which is being presented in the Dissertation entitled **"Heat Transfer and Friction Factor Characteristics of Double Pass Solar Air Heater Having W-Shaped Artificial Roughness on Absorber plate"** in partial fulfillment of the requirement for the award of degree of **Master of Technology** and submitted in Department of Mechanical Engineering, Lovely Professional University, Punjab is an authentic record of my own work carried out during period of Dissertation under the supervision of **Mr. Sudhanshu Dogra**, **Assistant Professor**, Department of Mechanical Engineering, Lovely Professional University, Punjab.

The matter presented in this dissertation has not been submitted by me anywhere for the award of any other degree or to any other institute.

Date: **(Manish Kumar Tated)**

This is to certify that the above statement made by the candidate is correct to best of my knowledge.

Date: (**Sudhanshu Dogra**)

The M-Tech Dissertation examination of Manish Kumar Tated, has been held on date _____

Signature of Examiner

ACKNOWLEDGEMENT

This Dissertation was a welcome and challenging experience for me as it took a great deal of hard work and dedication for its successful completion. It's my pleasure to take this opportunity to thank all those who help me directly or indirectly in preparation of this report.

I Manish Kumar Tated student of Lovely Professional University, in my acknowledgement, I would like to thank all the people who have helped me in making this project a success. My first and foremost acknowledgement goes to my mentor Mr. Sudhanshu Dogra for the assistance and guidance that he provided throughout the session. I am ever grateful to him for that. I want to say special thanks to Mr. Sundeep Singh for helping me a lot in the completion of dissertation.

I am also thankful to my university which assigned me this project which immensely improved our technical knowledge. I am thankful to university for providing me various resources like lab, tools for the timely completion of this project.

There times in such projects when clock beats you again and again and you run out of energy and you want to finish it once and forever. Last but not the least I would like to thank family and friends for their boost and support in every sphere. Their vital push infused a sense of insurgency in me.

I thank you one and all.

Date:

Manish Kumar Tated

Regd. No.: 11004227

Lovely Professional University

TABLE OF CONTENTS

LIST OF TABLES

LIST OF FIGURES

ABSTRACT

In view of present day sources of producing energy and their depletion rate, there is a large shift of attention on using non-convention sources of energy so that the conventional one‘s can be sustained. Similarly, heating for any process requires larger power input in order to serve for various purposes like food dehydration, space heating etc. Hence there is a need to concentrate on effective utilization of energy available naturally.

The present work is an attempt to increase the thermal performance of solar air heater. Solar air heater is widely used in industrial as well as domestic applications like crop drying, curing of industrial products and drying of concrete, clay building products. Poor efficiency is the major problem of conventional solar air heater. Efficiency of solar air heater can be improved by making it double pass. DPSAH is more efficient than SPSAH. In double pass solar air heater (DPSAH) the fluid passes through both sides of absorber plate. Heat transfer through DPSAH can be enhanced by many ways like using extended surface, porous media, corrugated surface or artificial roughness on absorber plate. Use of artificial roughness on absorber plate is most competent method to enhance the thermal performance of DPSAH in terms of cost and suitability. This work advocates about the use of new roughness geometry i.e. W-shaped on absorber plate of DPSAH and how the change in roughness and flow parameter affects it’s heat transfer and friction factor characteristics in order to obtained optimize orientation of W-shaped artificial roughness. A comparison is drawn between smooth absorber plate and W-shaped roughened absorber plate for the output behavior of DPSAH.

NOMENCLATURE

A	Area of cross-section, m^2
A_c	Surface area of collector, m^2
A_o	Throat area of orifice plate, m^2
C_d	Coefficient of discharge for orifice meter
C_p	Heat of air at constant pressure, kJ/kg K
D_h	Equivalent diameter of the air passage (hydraulic diameter)
e	Roughness height, m
e/D_h	Relative roughness height
f	Friction factor
H	Height of air channel, m
W	Width of air duct, m
h	Convective heat transfer coefficient, W/m^2-K
k	Thermal conductivity of air, W/m-K
L	Duct length for calculation of friction factor, m
m	Mass flow rate of air, kg/s
Nu	Nusselt number
P	Pitch
p/e	Relative roughness pitch
W/H	Channel aspect ratio
Re	Reynolds number

Greek symbols

α	Rib angle of attack, degree
β	Ratio of orifice diameter to pipe diameter
ρ	Density of air, kg/m^3

CHAPTER 1 INTRODUCTION

1.1 Overview

The most common term to measure all types of work done by nature and humans is Energy. Everything occurs in the world is the conversion of energy from one form to another form. Maximum peoples used the term energy for contribution to their bodies or input to the machines.

Different categories of energy sources

1. **Primary Energy Sources**: The primary energy sources provide net flow of energy. Oil, coal uranium are examples of this type. They can produced energy during combustion is much higher than what energy required to obtain these fuels. Yield ratio of energy is very high.
2. **Secondary Energy Sources**: They produce no net energy. Their yield is less than the input. Solar energy, hydraulic energy and wind energy are some example of this type.
3. **Supplementary Energy Sources**: The net energy yield of these energy sources is zero. In terms of energy they require highest investment. Thermal insulation is an example of this type. [15]

Future of World Energy If the present trend continues, the world will be very crowded in the coming years. The conventional energy sources like coal, petrol are depleting very fast whereas nuclear energy requires a lot of skilled technicians and safety against nuclear radiations. Also these are not good for health as they produce a lot of pollution and harm our body. So there is a need of switching over to non-conventional sources of energy like solar energy, geothermal energy and wind energy. These are non-exhaustible types of energy sources and produce no pollution. The different sources of energy in percentage consumed by the world is given in "Table 1". "Figure 1.1" shows the graphical representation of % energy utilization.

Table 1.1 % Utilization of energy sources consumed by the world

Energy Sources	% Utilization	Energy Sources	% Utilization
Oil	38.3%	Hydro	2.0%
Coal	32.5%	Dung	1.2%
Gas	19%	Waste	0.3%
Wood	6.6%	Uranium	0.13%

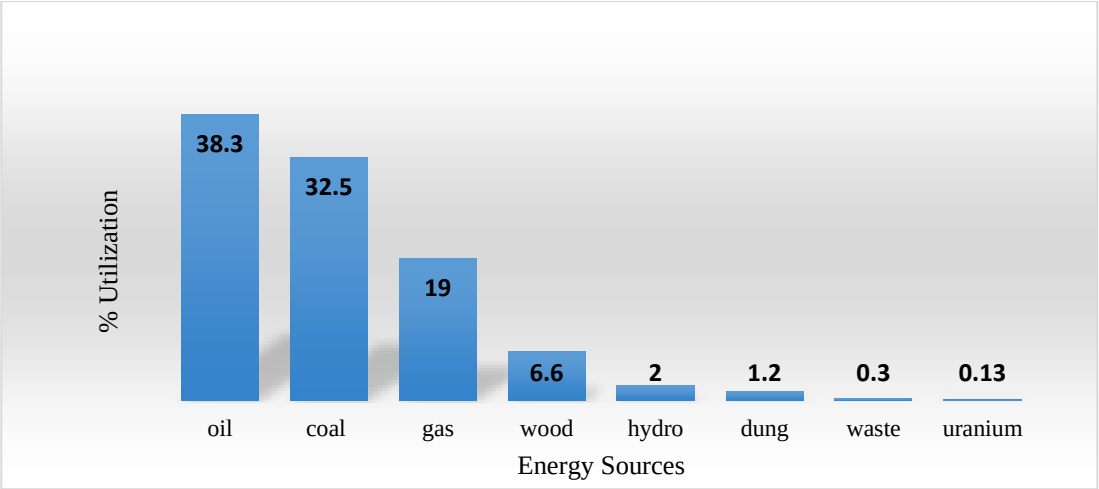

Figure 1.1 Bar chart for % Utilization of energy sources consumed by the world.

Commercial energy sources: Oil, coal, gas, uranium, hydro are used 92%.

Noncommercial sources: wood, dung and agriculture waste are used 8% only.

1.2 Non-conventional sources

"Alternative" "appropriate" "natural" are some of the generic terms used to describe the whole range of technologies designed to tap the earth's natural energy flow.

1.2.1 Solar energy

Sun is the major source of energy, it stores around 178 billion MW potential. This solar potential is around 20000 times more than today's energy demand of whole world. Due to some difficulty this solar energy could not be utilized on large scale. Solar energy can be used as photovoltaic or thermal. Solar energy as thermal is being used for steam and hot water production.

1.2.2 Wind energy

Wind energy developed by high wind velocity. In whole world about 0.7 million wind pumps are in action. A wind speed of 3 m/s is needed to run the wind turbine. This is considered to have high efficiency.

1.2.3 Geothermal energy

Geothermal energy is thermal energy which is stored and generated in earth. Geothermal energy derives the heat from the center of the earth. Approximately 700 MW of power is produced by geothermal energy in China and Philippines.

1.2.4 Tidal energy

Energy from seas can be utilized as wave, tidal or ocean thermal energy. Little amount of energy we get by this source.

1.3 Solar Energy

We get a huge amount of energy from Sun. The earth interrupted around 1.8×1011MW energy, which is exhausted by Sun. This amount of energy is approximately 20000 times more than present conventional source of energy consumption rate. Due to this reasons all the energy needs of human beings in present as well as in future could be supply by solar energy. This unique property makes the solar energy as a most accomplished renewable source of energy. [32]

The efforts have been made to make use of the solar energy emitted by the sun (approx. 1000W/m^2) in steam production. This steam drives the prime movers for the generation of electrical energy. However there is limited application of solar energy in the electrical power generation due to availability of solar energy is not uniform.

Solar energy is the best substitute for generation of power in present and future, because a huge amount of energy we obtain from sun is many times more than present consumption rate. The average intensity of solar radiation in India works out to be approximately 2000 kWh/m^2 as compared to the world average of 2500 kWh/m^2. But of the total solar energy reaching the earth's surface only 7-8% is being used, so there is a need to explore it and use it in a more efficient way.

1.3.1 The applications of solar energy

1. In Solar furnaces.
2. In steam generation.
3. For dehydration of animal and agricultural products.
4. In cooling and heating of building.
5. For production of salt by evaporating the sea water.
6. For heating of water.
7. Solar distillation.
8. In solar engines for pumping of water.
9. Solar cookers.

In general, sun's energy is the term refers to the energy produced and radiated by the sun. Humans utilized the energy in the form of heat or electricity, so by directly or indirectly methods solar energy could be converted in the most suitable form of energy.

The major problems in utilization of solar energy are:

1. The variable and irregular way of solar energy to reach earth's surface.
2. A large area is needed to collect the energy exhausted by sun.

1.3.2 SWOT Analysis of Solar Energy

A SWOT analysis is an organized preparation method. In this analysis 'S' tends for strength, 'W' tend for weakness, 'O' tends for opportunity, and 'T' tend for threats. A SWOT analysis recognizing the external and internal factors that are advantageous and disadvantageous to attain desired objective.

1.3.2.1 Strength

1. Never ending source of energy.
2. Pollution free.
3. Scope for decentralization.
4. Easy to operate.
5. Saves fossil fuel deposits.
6. Less hazardous.
7. Can be utilized in any form of energy.

1.3.2.2 Weakness

1. Problem for storage.
2. Not available in cloudy or eclipse days.
3. Initial investment is high.
4. Needs subsidy.
5. Spares not easily available.
6. Quantum varies according to seasons or weather.
7. Not yet taken on priority list.

1.3.2.3 Opportunity

1. Scope for utilizing magnetic energy from solar wind.
2. Chance of hazard is less.
3. Scope for decentralization.
4. Totally pollution free.
5. Vast opportunity for expansion in many uses.

1.3.2.3 Threat

1. Threat from oil lobby.
2. Threat from coal lobby.
3. Opposition from different forces due to subsidy.
4. Fluctuations due to season or weather may discourage consumers.

1.4 Solar Constant

The sun is very large sphere, which contains a verity of hot gases. The various types of fusion reaction occur inside the sun which produces heat in sun. This heat reaches the earth's surface in the form of solar radiation.

Some calculated data are as follows:

1. Diameter of sun=1.39×10^6 km
2. Diameter of earth=1.27×10^4 km
3. Mean distance between sun and earth =1.50×10^8 km
4. Angle subtend by sun at earth's surface = 32minute

The intensity of solar radiation varies from its center to its edges. The NASA (National Aeronautics and Space Administration) expressed standard value of the solar constant as follows:

1. 1.353 kilowatts per square meter.
2. 429.2 BTU per square feet per hour.

1.4.1 Component of Solar Radiation

The main components of solar radiation are direct or beam radiation, diffuse radiation and reflected radiation.

1.4.1.1 Direct or Beam Radiation (I_b)

A solar radiation that reaches the ground directly from the sun without absorbed or dispersed is called direct radiations. When an opaque body interrupt the direct radiation, then a shadow is produces.

1.4.1.2 Diffuse Radiation (I_d)

Some part of the solar radiation is absorbed by the water vapor and air, which is present in atmosphere. When it passes through atmosphere, by collision of dust particles and water vapor some part of radiation scattered. This scattered and absorbed part of solar radiation reaching the earth surface is termed as diffuse radiation.

Global radiation (I) is the sum of direct radiation (I_b) and diffuse radiation (I_d), expressed as:

$$I = I_b + I_d \qquad (1.1)$$

1.4.1.3. Reflected Radiations (I_r)

Some part of the solar radiation is reflected by atmosphere and earth's surface, this part of radiation is termed as reflected radiation.

1.5 Solar Collectors

The solar collector collects the solar energy, absorber plate of solar collectors absorbs the heat and transmit this heat to the fluid which comes in contact with absorber plate. The absorber component of solar collector is an essential component, which converts the solar energy into thermal energy. These collectors are categories mainly 2 types:

1. Flat plate or Non-concentrating type solar collector.
2. Concentrating type solar collector.

Flat plat collector are those collector, in which area of absorption is same for interruption as solar radiations emits on collector surface. But the concentrating type collectors focus the beam radiation on to a receiving area and usually have concave reflecting surface to intercept, it increases the radiation flux significantly. Radiation is collected by this type of collectors is hundred times greater than the flat plate collector.

Table 1.2 Different Solar collectors and their working temperature range.

S. No.	Collector type	Working temperature range (°C)	Concentration Ratio
1.	Non concentrating collector	≤ 80	1
2.	Fixed concentrating collector	80-130	4-6
3.	Parabolic trough concentrating collector	130-300	10-100
4.	Parabolic dish concentrating collector	300-700	100-400
5.	Central concentrating collector	600-1000	400-3000

1.5.1 Flat Plate Collectors or Non-Concentrating Solar Collectors

Flat plate collectors are particularly suitable, when temperature required below than 90°C. Water heating and space heating are some application of this type of collector. Flat plate collectors are made in rectangular panels, from 1.7 to 2.9 m^2 in area and comparatively simple in construction. It can accumulate both direct and diffuse solar radiations. A flat plate collector contains a flat surface called as absorber plate having high absorptivity for solar radiations. Generally absorber plate is a metal plate painted with black color to absorb the solar radiations. Energy is carried away from the absorber plate by a heat transfer medium like air and water, flowing across the collector. A transparent glass cover is used at top side of the collector, which transmits shorter wavelength solar radiation on absorber plate.

The main components of the flat plate collector are

1. One or more transparent glass cover.
2. Tubes, fins, passage or channels which carry the fluid.
3. The metallic absorber plate having black surface.
4. Thermal insulation, to reduce the losses through collector.
5. A container, which encloses all the components and guards them from the climate.

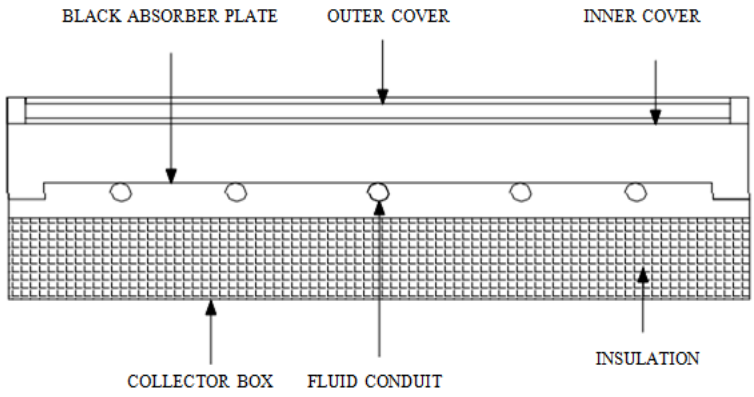

Figure 1.2 Flat plate or non-concentrating type collector.

There are 2 types of flat plate collector on the basis of heat transfer to fluid. First type of flat plate collector provides heat to the air and other type provide the heat to the liquid flowing through it.

1.5.1.1 Air Heating Flat Plate Collectors

Due to simplicity and cheap Air heating collectors widely used as collection devices. It is suitable for seasoning of timber, in industrial products curing and space heating. As shown in "Figure 1.3", the glass allows the solar radiation to falls on absorber plate of collector, which is black painted for better absorption. Then absorber plate is heated up and the heat energy generated there is carried away by the air, flowing beneath the absorber plate.

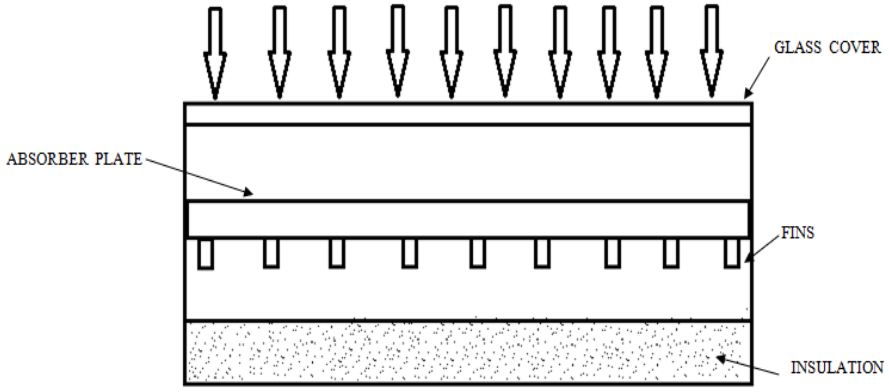

Figure 1.3 Air heating flat plate solar air collector.

1.5.1.2 Liquid heating flat plate collectors

This type of flat plate collector contains a high absorptivity absorbing surface for solar radiation i.e. metal plate like Cu, Al and steel with tubing of cu in contact with absorber plate. From the storage tank the liquid is inserted into Cu tubes. Then the heat of absorber plate is absorbed by the liquid flowing in tubes and return again in storage tank.

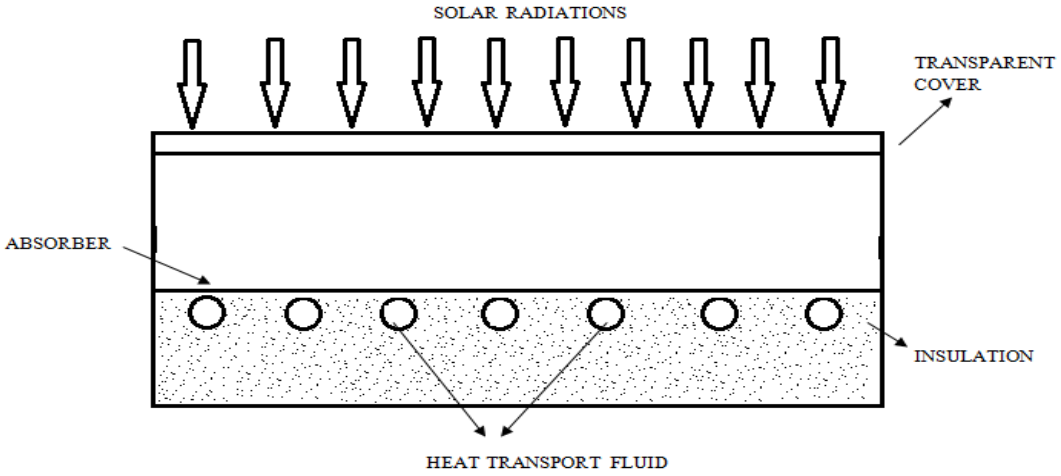

Figure 1.4 A typical liquid heating collector.

Advantages of flat plate collector:

1. Orientation towards the sun does not affect its performance.
2. It requires less maintenance.
3. Simple in construction.

Efficiency of flat plate is very less so that it is drawback.

1.5.2 Focusing Collectors

For many applications higher temperatures that obtained from flat-plate Collectors are desirable to deliver energy. The delivery temperature can be increased up to a certain level by minimize area of heat losses. In order to minimize the losses between the solar radiation source and absorbing surface of collector an optical device is fitted. At the same absorber temperature concentrating collector have less heat losses compared to a flat-plate collector. Due to this reason, concentrating collector collects the solar radiation from large area and concentrate these radiation on a point. Parabolic mirror are used for this objective. The focusing collector absorbs the radiation, which having high intensity.

Reflectors are used as an optical system for focusing collectors. It is nothing but a modified form of flat plate collector. A concentrator inserted between the source of solar radiation and absorber plate of collector. Thus a focusing collector consists of parabolic and cylindrical or spherical receiver as shown in “Figure 1.5”

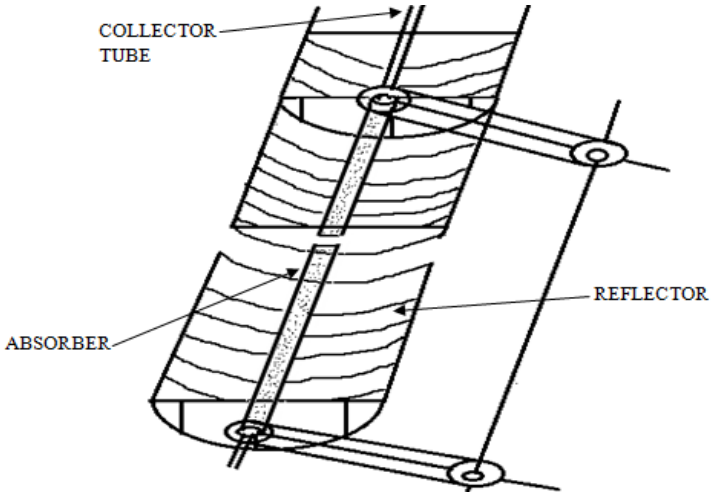

Figure 1.5 A Parabolic or concentrating type of collector.

1.6 Solar Air Heaters

In many energy conversion system, the heat transfer medium is air. A variety of designs for solar air heaters present today. The absorber plate of the solar air is in different form like corrugated metal absorber plate, smooth GI sheets, black painted glass plates etc.

1.6.1 Simple Flat Plate Collector

It is the basic and simplest form of solar collector. It contains one or more glass cover (glazing) above the absorber plate. Insulation is provided to reduce the losses. Air passes through the collector either above or below the absorber plate. “Figure 1.6” shows the pictorial view of it.

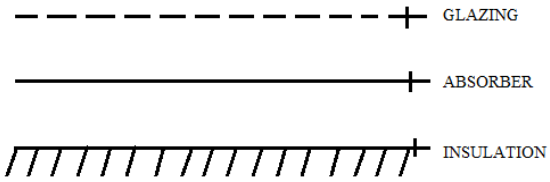

Figure 1.6 A flat plate collector.

1.6.2 Finned Plate Collector

As we know heat transfer coefficient between flowing fluid and absorber plate. Fins are using in finned plate collector to enhance the heat transfer coefficient. In the flow path of air the fins are usually attached as shown in “Figure 1.7”

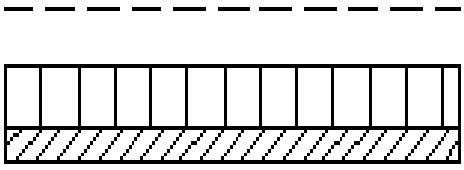

Figure 1.7 A Finned plate collector

1.6.3 Corrugated Plate Collector

Corrugated flat plate collector is also a modified form of flat plate collector. The absorber plate of this types corrugated in rounded trough or v-troughs. Heat transfer area increases by using corrugated geometry. The front view of this type is shown in "Figure 8"

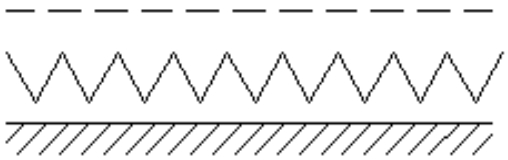

Figure 1.8 Corrugated plate collector.

1.6.4 Matrix Type Collector

In this type of collector between glazing and absorber plate in flow path of air an absorbing matrix is positioned. The material of matrix can be cotton gauge, expanded metal plate or loosely packed porous material. It gives high heat transfer to volume ratio as well as low friction losses depending upon the design as shown in Figure

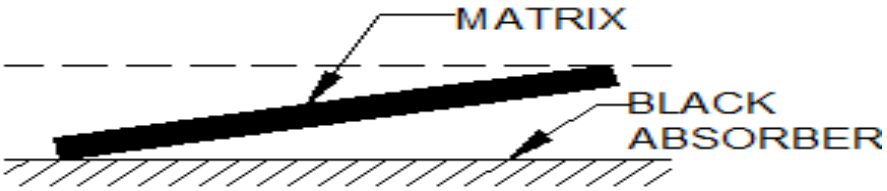

Figure 1.9 Matrix type collector.

1.6.5 Two-Pass Solar Air Heater

For reducing the heat losses from top of the collector double pass solar air heater is used. The air firstly passed between the covers of a two glass cover heater and then under the absorber plate. So by this outlet glass shelter temperature was lowered by 4-5°C. The losses were reduced, by using this concept. The efficiency of the increased by 10 to 15% higher than the single pass air heater.

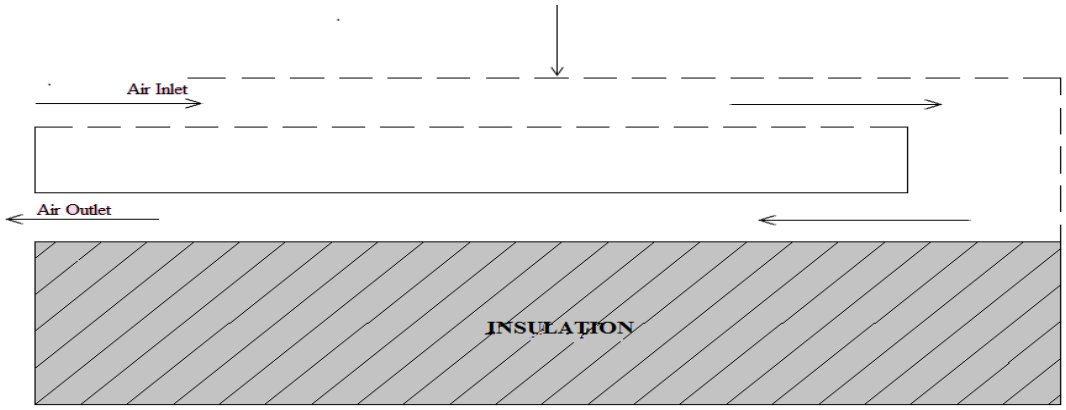

Figure 1.10 Two pass solar air heater.

CHAPTER 2 TERMINOLOGY

2.1 SPSAH and DPSAH

Single Pass Solar Air Heater (SPSAH): In single pass configuration, air passes on one side of absorber plate. The absorber plate uniformly heated by solar energy. Due to conductive properties of absorber plate and convective properties of air heat is transferred from absorber plate of solar air heater to the moving air.

Double pass Solar Air Heater (DPSAH): In double pass configuration of solar air heater, air passes through both upper and lower section of the absorber plate. Due to significant pressure drop, for circulation of air pumping power is required. DPSAH is more efficient than SPSAH.

2.2 Roughness and Flow Parameters of Roughness Ribs

Roughness geometry and flow parameters are important ingredients in present study. The roughness geometry is governed by 4 dimensionless parameters, which is aspect ratio (W/H) of duct, relative roughness height (e/D_h), relative roughness pitch (p/e), and inclination angle of ribs (α). Where 'e' is the diameter of the artificial roughness ribs, which is circular in shape and diameter of the ribs is 2mm. A short description on these roughness geometries parameter as follows:

2.2.1 Roughness Parameters

1. Aspect ratio (W/H): The duct of double pass solar air heater is rectangular. Width to height ratio of the duct is termed as aspect ratio of duct. Width of duct is 250mm and height of duct is 25mm. Aspect ratio (W/H) of duct is fixed as 10.

2. Relative roughness pitch (p/e): Term pitch (p) is distance between two successive ribs and e is the diameter of the circular ribs. Ratio of pitch (p) to diameter of rib (e) is termed as relative roughness pitch (p/e). It is an important parameter which decides the geometry of roughness ribs. The relative roughness pitch for present study ranges from 5 to 20.

3. Relative roughness height (e/D_h): Another important term which decides the geometry of roughness element is relative roughness height (e/D_h). It is the ratio of ribs diameter to hydraulic diameter (D_h) of duct.

4. Angle of attack (α): Inclination of ribs with respect to horizontal plane is termed as angle of attack (α). It is also an important parameter which decides the geometry of roughness element. Type of flow depends on inclination of the ribs.

2.2.2 Flow Parameters

1. Mass flow rate (m): By using measured pressure drop across the orifice meter mass flow rate is calculated by

$$m = C_d A_0 \sqrt{\frac{2\rho\Delta P_0}{1-\beta^4}} \quad (2.1)$$

2. Reynolds number (Re): Reynolds number of airflow is calculated by knowing velocity, density, hydraulic diameter of duct and viscosity. Reynolds number is important parameter which decides the turbulence of air through duct. If Re ≥2300 then flow is turbulent. Re is calculated by

$$Re = \frac{\rho V D_h}{\mu} \quad (2.2)$$

Where D_h is the hydraulic diameter and calculated by

$$D_h = \frac{4A_C}{P} \quad (2.3)$$

Some other terminologies are as follows:

1. Heat transfer coefficient (h): It is calculated by knowing the plate temperature and area of heating surface. Heat transfer coefficient is important parameter, which decides the heat transfer characteristics. It is calculated by

$$h = \frac{Q_u}{A_p(T_p - T_f)} \quad (2.4)$$

2. Nusselt Number (Nu): The Nusselt number (Nu) defined as ratio of convective heat transfer to conductive heat transfer. Nu is calculated by

$$Nu = \frac{hD_h}{k} \quad (2.5)$$

3. Friction factor (f): Darcy Wiesbach equation is using to calculate friction factor by measuring pressure drop in test section. Friction factor decides the pressure drop in test section and pumping power, calculated by

$$f = \frac{2(\Delta P)D_h}{4\rho L V^2} \quad (2.6)$$

4. Thermal efficiency (η_{th}): Ratio of heat gained by air through absorber plate to heat given to the absorber plate is termed as thermal efficiency. η_{th} Given by

$$\eta_{th} = \frac{Q_u}{IA_p} \tag{2.7}$$

Where $Q_u = mC_p(T_o - T_i)$, heat gained by air

5. Thermohydraulic efficiency (η_{eth}): It is the effective efficiency of solar air heater which includes the effect of pumping power. Thermohydraulic efficiency is calculate by taking ratio of actual heat gained by air to total heat given to the solar air heater system. η_{eth} Calculated by

$$\eta_{eth} = \frac{Q_u - \frac{P_m}{C}}{IA_p} \tag{2.8}$$

Where P_m is the mechanical power and C is correction factor.

CHAPTER 3 REVIEW OF LITERATURE

The purpose of comprehensive review of literature is to produce information on the issues to be considered in present study. This chapter includes the effective methods opted by previous researchers in order to enhance the heat transfer through solar air heater. These methods includes using porous media, using extended surface like fins, corrugated surface and by using artificial roughness ribs. Surface roughness created by artificial roughness ribs is the best suitable method to enhance the heat transfer to air by absorber plate in terms of cost and suitability also.

3.1 Concept of Artificial Roughness on Absorber Plate

The main problem with conventional solar air heater is low heat transfer rate due to laminar sublayer, which is present in turbulent boundary layer. So all the heat is not able to reach the absorber plate. It is necessary that flow should be turbulent just above the heat exchange surface.in Heat transfer coefficient would be higher by turbulent flow over absorber plate. However, the blower or fans are used to create such type of turbulence. Excessive turbulence means excessive power required for creating turbulence, so minimize this power loss to make it more efficient.

A small laminar sublayer always present in turbulent boundary layer, this sublayer creates high confliction to heat flow. By using the roughness ribs, this laminar sublayer breaks down and more turbulence generates near the absorber plate. Due to roughness ribs heat transfer rate and friction factor increases. Hence, turbulence should be create just above the heat transfer surface i.e. absorber plate.

If flow disturbed, there will be more friction losses. To avoid the losses from friction, flow should not too much disturbed. As compare to duct dimension, height of the roughness element should small for less friction losses. Diameter of the ribs (e) and pitch (p) are most important parameter for roughness geometry. There are 3 major dimensionless parameters which decide the geometry of artificial roughness ribs, as follows:

1. Relative roughness height (e/D_h)
2. Relative roughness pitch (p/e).
3. Angle of attack (α).

The roughness elements are present in two dimension as well as in three dimension. Ribs geometry can be V-shaped, W-shaped, inclined, transverse or discreet form. Ribs can be circular, square, semicircular or grooved cross section, but most commonly circular shaped ribs are used. [28] To see the effect of this artificial roughness on heat transfer characteristics, many investigators

experimentally investigate to search the most efficient orientation of the roughness geometry and best dimension of ribs element is discussed in later section of this chapter. Some most common roughness geometry and their dimensional parameter is given in "Table 3.1".

Table 3.1 Different roughness geometry and roughness parameters.[15]

S. No.	Geometry	Investigator	Roughness Parameter
1.	Continuous transverse ribs	Prasad & Saini	(p/e), (e/D_h)
2.	Transverse ribs	Verma & Prasad	(p/e), (e/D_h)
3.	Continuous inclined ribs	Gupta, Solanki & Saini	(p/e), (e/D_h), α
4.	V-shaped discrete ribs	Muluwork, Saini & Solanki	(e/D_h), α, (B/S)
5.	Chamfered-shaped ribs	Karwa, Solanki & Saini	(p/e), (e/D_h), (W/H)
6.	V-shaped continuous ribs	Momin, Saini & Solanki	(p/e), (e/D_h), α
7.	Wedge shaped ribs	Bhagoria &Saini	(p/e), (e/D_h), ⍉
8.	Dimple shaped ribs	Saini & Verma	(p/e), (e/D_h)
9.	Metal grit ribs	Karmare & Tikekar	(p/e), (e/D_h), (L/s)
10.	Combination of discreet transverse & inclined ribs	Varun, Saini & Singal	(p/e), (e/D_h), α
11.	Discreet W-shaped	Kumar, Bhagoria & Sarvia	(p/e), (e/D_h), α
12.	M-shaped ribs	Chaudhary, Varun & Chauhan	(p/e), (e/D_h), α

3.2 Flow Pattern of Fluid over Absorber Plate

In this section flow pattern of fluid over absorber plate will be discussed. The effect of roughness parameter on flow of fluid, generation of flow separation, concept of reattachment affect the flow pattern of fluid. The detail description for the effect of roughness parameter on flow pattern as follows:

3.2.1 Effect of Roughness Element (Rib)

Due to presence of ribs on the absorber plate, on both sides of ribs flow separation region is formed. Because of flow separation, there are vortices forms over absorber plate. Due to the formation of these vortices, turbulence is generated which increases heat transfer and friction factor.

3.2.2 Effect of Relative Roughness Pitch (p/e) & Relative Roughness Height (e/D_h)

Prasad and Saini [25] had been shown the effect of height of the ribs on sublayer. "Figure 3.1" shows the effect of relative roughness pitch (p/e) on flow pattern over absorber plate. "Figure 3.2" shows the effect of relative roughness height (e/D_h) ratio on flow pattern. While being downstream of a rib the flow get separated but does not get reattached if the relative roughness pitch is less than 10. The maximum amount of heat transfer occur near the reattachment point. Heat transfer also gets enhanced by reducing the relative roughness pitch (p/e) ratio for constant (e/D_h) ratio or vice versa. The optimum p/e ratio and e/D_h ratio can be find out by observing the effect of this parameter on flow pattern.

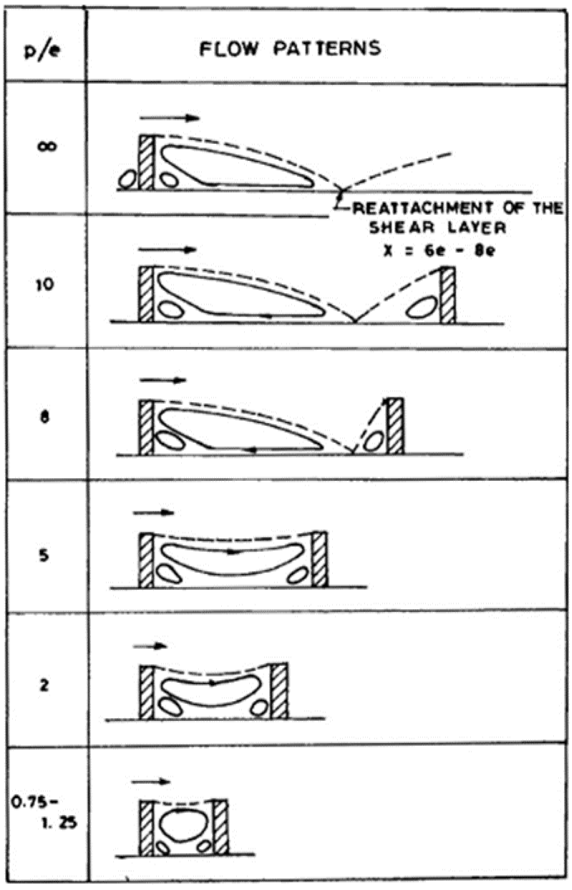

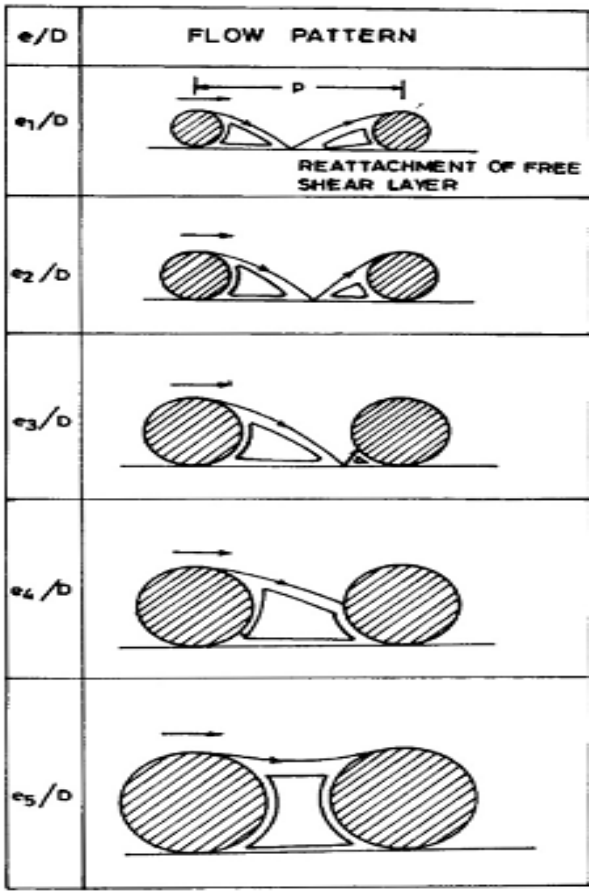

Figure 3.1 Effect of p/e ratio on flow pattern

Figure 3.2 Effect e/D_h ratio on flow pattern.

"Figure 3.3" shows the effect of height of the ribs on laminar sublayer. If the height of the ribs increases flow will unduly disturbed, which causes friction losses. By observing these roughness parameter effect on flow parameter an optimum dimension for the ribs geometry can design. Effect of ribs inclination or ribs angle is discussed in next part of this chapter.

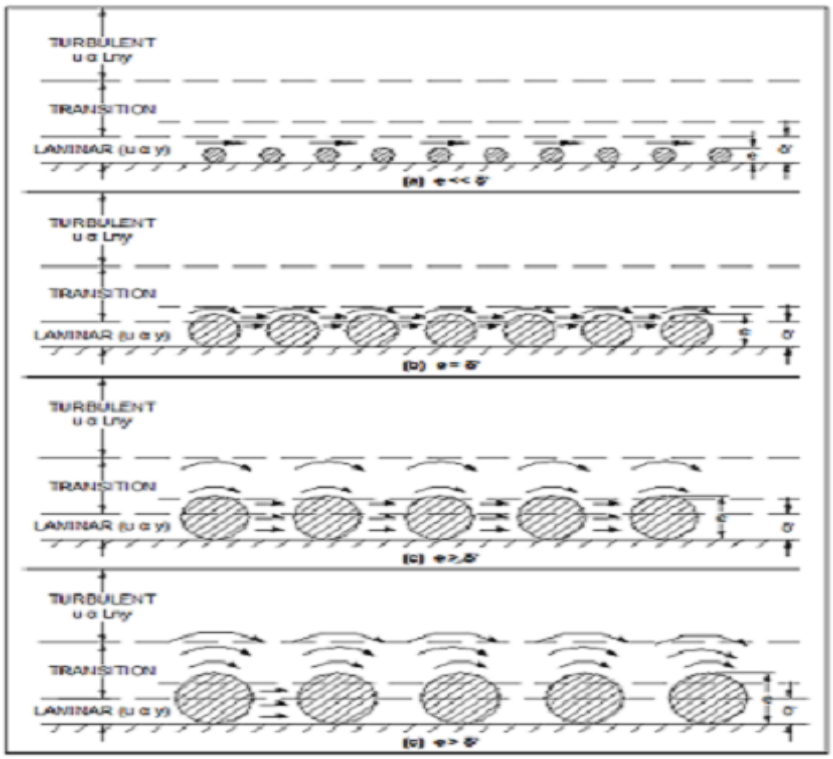

Figure 3.3 Effect of rib height on laminar sublayer

3.2.3 Effect of Rib Inclination

The inclination of rib is responsible for the substantial length wise deviation in the heat transfer coefficient, this is due to the formation of span wise anti rotating secondary flow. It has been found that the secondary flow which generates immediately join the main stream. The fluid moving from leading edge of the rib to the trailing edge of the rib is the main stream. Enhancement in heat transfer occur when the secondary flow bring the cooler channel in contact with the leading edge of the rib while the heat transfer at the trailing edge is comparatively low.

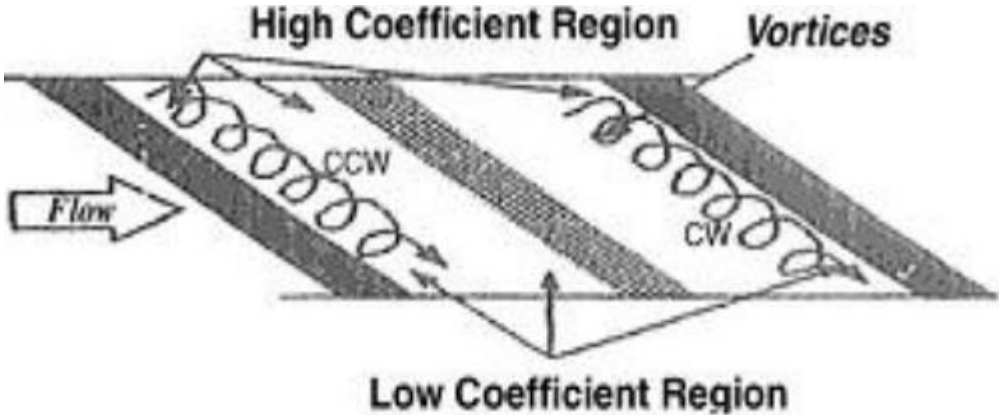

Figure 3.4 Effect of inclination of ribs on flow pattern.

3.2.4 Effect of V-Shaping of Rib

Formation of V using rib forms the two leading edge where rate of heat transfer is high and one trailing edge where rate of heat transfer is low [36]. Overall heat transfer coefficient gets increased as the secondary flow occurs in both leading edges as compare to straight inclined rib. As in this case secondary flow gets developed at both the leading edges as compared to inclined ribs where secondary flow gets developed at only one leading edge hence V- ribs are generally more efficient than the inclined ribs and results in better enhancement of heat transfer coefficient than inclined ribs.

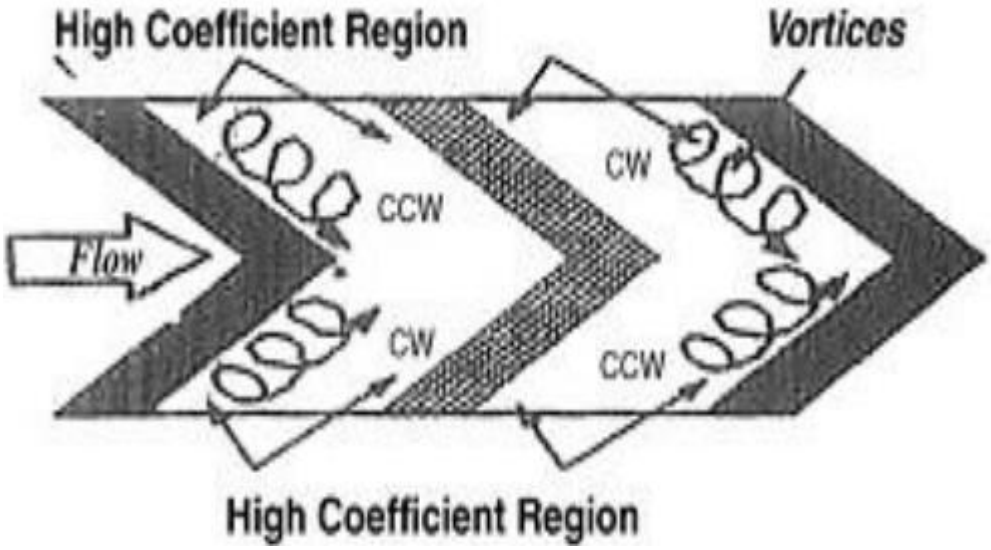

Figure 3.5 Effect of V-shaped ribs on flow pattern

3.2.5 Effect of Rib Cross-Section

Level of the flow disturbance and the size of separated region are affected by rib cross-section. Circular cross-section has less friction factor as compared to rectangular and square cross-section on account of reduced separated region. Rate of heat transfer is affected very badly due to fall in flow disturbance level because of diminished size of separated region [29]. It means that more the cross sections of the ribs more will be the heat transfer coefficient and lesser will be the power loss.

By observing these roughness parameter effect on flow parameter an optimum dimension for the ribs geometry can design. The literature survey for single pass and double pass solar air heater is presented in next section of this chapter, which included theoretical as well as experimental investigation done by researcher in order to find out the enhancement technique of thermal performance of solar air heater.

3.3 Literature Review

3.3.1 Single Pass Solar Air Heater

Prasad et al. [25] studied the effect of relative roughness pitch (p/e), relative roughness height (e/D_h), and Reynolds number on heat transfer and friction factor. They observed that near the reattachment point maximum heat transfer occur. When the roughness height is higher than the laminar sub layer the goal of optimal thermo hydraulic performance is accomplished.

Nusselt number was observed 2.38 times more than smooth plate and friction factor was observed to be 4.25 times that of smooth duct. Maximum heat transfer enhancement occur at e/D_h ratio of 0.033 and p/e ratio of 10. They have also developed the correlation for friction factor and Stanton number.

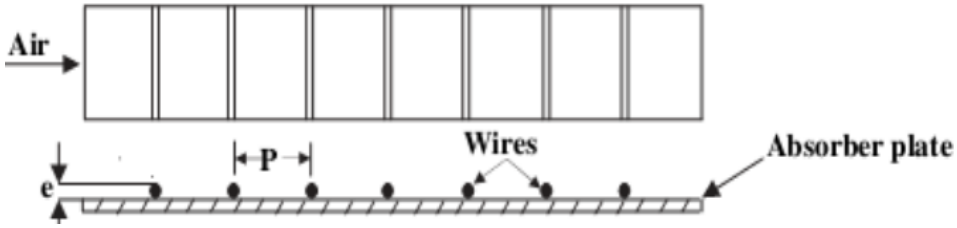

Figure 3.6 Absorber plate with circular ribs

Gaurav Bhardwaj et al. [14] showed the effect of inclined continuous ribs on thermal performance and friction characteristics of solar air heater having equilateral triangular duct. The parameter used by them as angle of attack (α) ranges from 30^0-60^0, Reynolds number varies from 4000-12000. They discussed the effect of roughness parameter on heat transfer and friction factor. Thermohydraulic performance also found by them for given range of parameters.

They observed that the maximum Nusselt number and friction factor arises at p/e ratio of 12 and 8 respectively, at an 60^0 angle of attack. They also observed that maximum thermohydraulic efficiency occurs when p/e ratio is 12 and angle of attack is 60^0.

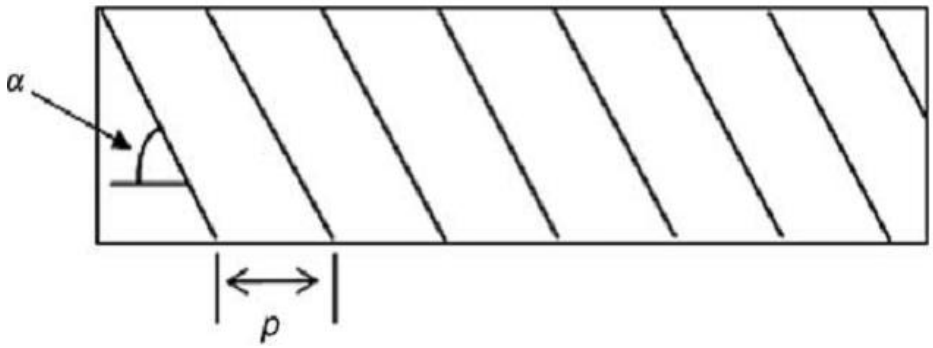

Figure 3.7 Schematic view of inclined ribs roughness geometry.

Sanjay Yadav et al. [27] investigation was based on to find out the effect of artificial roughness on heat transfer and friction factor of solar air heater having rectangular duct. Absorber plate was roughened by circular protrusion which was fixed on absorber plate in angular arc fashion. The range of roughness parameter were as follows, p/e ratio varies from 12 to 24, e/D_h ratio ranges from 0.015 to 0.03, arc angle (α) of protrusion taken as 45° to 75° and Reynolds number was varies from 3600 to 18100.

Based on experimental result they observed maximum enhanced heat transfer was 2.89 times and maximum enhanced friction factor was 2.93 times more than smooth one. At p/e ratio of 12, e/D_h ratio of 0.03 protrusion arc angle (α) of 60°, optimum heat transfer arises. Nusselt number and friction factor correlation they developed and maximum average deviation they found 3.81% for Nusselt number and 4.91% for friction factor respectively.

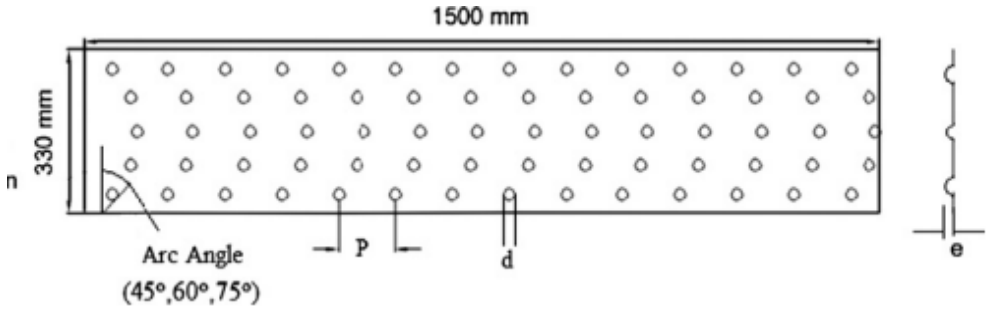

Figure 3.8 Arc shape protruded roughened absorber plate.

Abdul Malik et al. [2] experimentally studied the effect of V-shaped ribs attached to absorber plate of solar air heater on heat transfer and fluid flow characteristics. The range of flow parameters were encompasses as e/D_h ratio of 0.02-0.034, Reynolds number ranges from 2500-18000, and angle of attack (α) varies from 30° to 90° for a fixed p/e ratio of 10. They found Nusselt number and friction factor are more as compare to smooth plate. Maximum 'Nu' and 'f' was found to be 2.3 and 2.83 times of smooth plate at angle of attack (α) 60°. Correlations for Nusselt number (Nu) and friction factor (f) also derived by them.

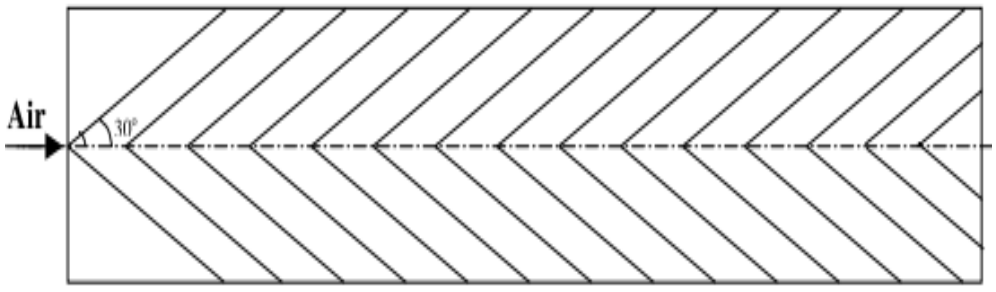

Figure 3.9 Schematic diagram of V-shaped roughened absorber plate.

Varun et al. [36] studied about the performance of solar air heater having combination inclined and transverse ribs on absorber plate. Reynolds number varies from 2000-14000 for experiment. Roughness parameter like p/e ratio varying from 3-8 and e/D_h ratio was fixed as 0.030. At p/e ratio of 8 they found the maximum thermal efficiency for solar air heater.

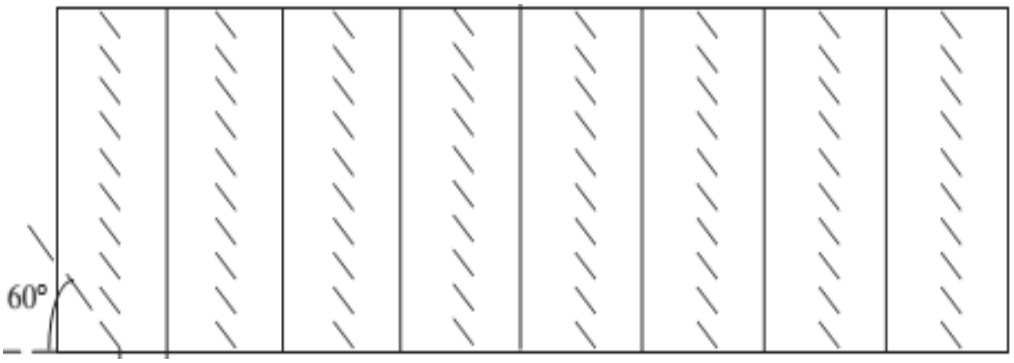

Figure 3.10 Absorber plate with combination of inclined and transverse ribs.

Sukhmeet Singh et al. [33] studied about the characteristics of discrete V-down shape roughness geometry. Reynolds number ranging from 3000-15000, relative gap width (g/e) varies as 0.5-2.0 and relative gap position (d/w) varies as 0.2-0.8. The e/D_h ratio, p/e ratio and ribs angle (α) in the range of 0.015-0.043, 4-12 and 30°-75° respectively. They found Nusselt number and friction factor was 3.04 and 3.11 times more than smooth plate respectively, at p/e of 10, α=60°, g/e=1 and d/w=0.65. They found variation in Nusselt number and friction factor 3.1% and 2.2% respectively by developing correlations.

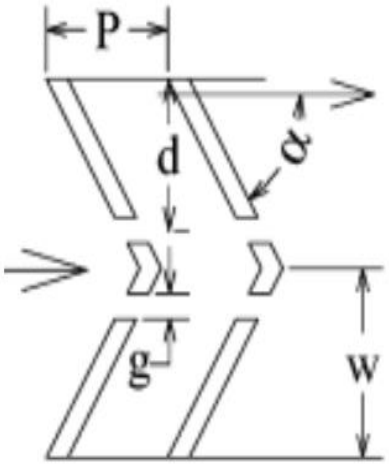

Figure 3.11 Configuration of discrete downward V ribs.

Bhagoria et al. [9] experimentally investigated the thermal characteristics of air heater having wedge shape roughened absorber plate. The various parameters which have been taken into account were

Reynolds number from 3000-18000, e/D_h ratio from 0.015-0.033, p/e ratio from 60$\backsim^{-1.0264}$ -12.12 and wedge angle from 8-15°. They found Nusselt number increases 2.4 times as that of the smooth duct and friction factor 5.3 times. Regression model for solar air heater developed by them.

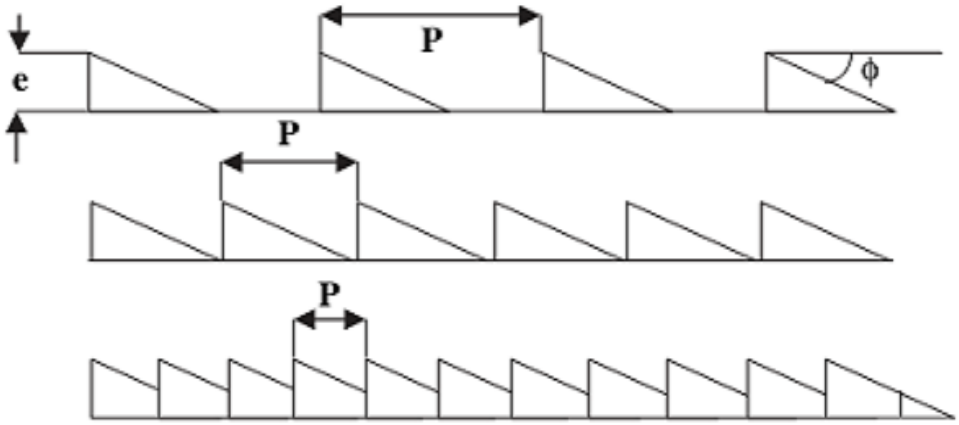

Figure 3.12 Configuration of wedge shape roughness

Lanjewar et al. [19] used the W-shaped ribs arrangement at different orientations on the absorbing surface of air heater. W-shaped ribs have been tested for both upstream and downstream flow. The various parameter which has been taken into account were W/H ratio of 8, p/e ratio of 10, e/D_h ratio of 0.03375, ribs angle (α) 30°-75°, Reynolds 2300-14000. They have been observed that as compare to W- up ribs, W- down ribs gives better efficiency. Maximum thermo hydraulic performance was 1.98 times for W- down ribs and 1.81times of smooth plate for W- up ribs. Regression model prepared by them to find out the correlation.

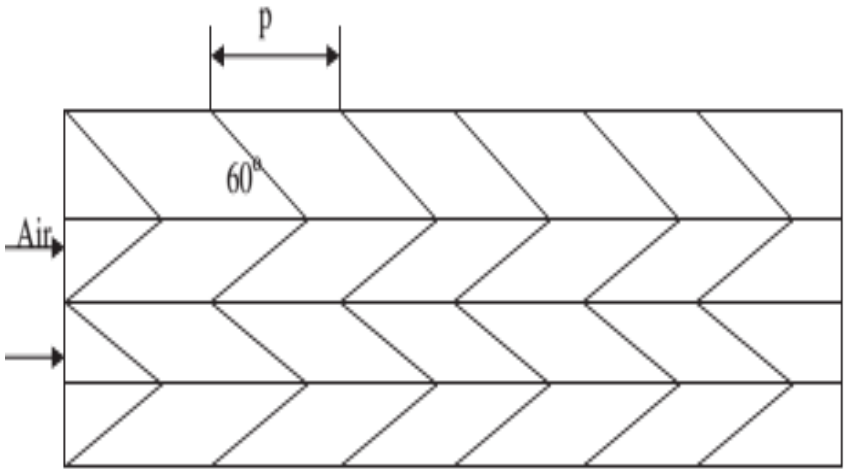

Figure 3.13 Schematic diagram of 60° W-shaped ribs

3.3.2 Double pass solar air heater

Suppramanium et al. [35] introduced the concept of two pass solar air heater. They found the performance of solar air heater depends on the losses from collector surface. By the use of suitable insulation the losses from bottom and sides of solar air heater can reduce. In order to reduce the losses from simple two- glass cover solar air heater, a different setup was constructed in which a passage was made to pass the air between glass panes before passing through collector plate. They observed outer glass cover temperature were significantly lower as well as efficiencies of the order of 10-15 % more as compare to conventional air heater.

Wijeysundera et al. [23] studied the method of improving the efficiency of solar air heater by using two covers in double pass mode. They found that it is an inexpensive method for improving the efficiency of solar air heater by 10 to 15 percent. They compared the performance of heat transfer model of solar air heater with single pass and solar air heater in double pass mode. By comparing the results of experimental data with predicted data they validated the computer models. Over a varied range of design and operating conditions collector performance were examined. They found that two pass design performs better than the single pass mode and for closed loop air circulation creates some problem in design of two pass mode of solar air heater.

Figure 3.14 Schematic view of two-pass collector

M.S. Sodha et al. [22] presented the concept of a non-porous double flow solar air heater in which air is driven on both side of the absorbing surface. They obtained expressions for heat flux and outlet air temperature by using parameters like mass flow rate of air, Distance along direction flow and other parameter. Double pass air heater found to be more efficient than Single flow air heater.

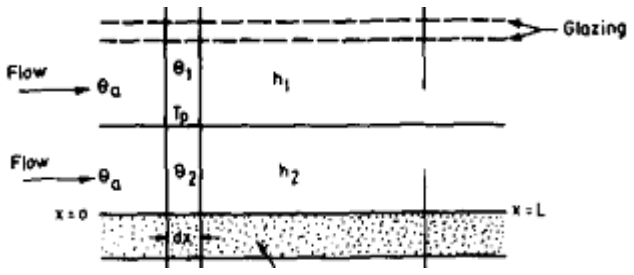

Figure 3.15 Configuration of double pass non-porous solar air heater

C. Chaudhary et al. [10] studied the ratio of annual cost and annual energy gain for two-pass solar air heater with single and double cover above the absorber. For a wide range of design and operational parameters they examined the cost-benefit ratios for solar collectors. They found that the for shorter duct lengths performance of two-pass air heater with single cover was most cost effective at lower mass flow rate of air.

H.M. Yeh et al. [17] studied experimentally as well as analytically the operation of double-flow solar air heater with fins attached on absorbing plate. They introduced the double-flow device in which heat transfer area doubled between the heated air and absorber plate. They found at same mass flow rate double-flow solar air heater with fins attached more efficient than single flow air heater. They investigate the effect of mass flow rate of air on collector efficiency and found that maximum thermal efficiency at mass flow rate of 0.5 kg/s. Optimum mass flow rate for best efficiency of finned air heater was 0.5 kg/s.

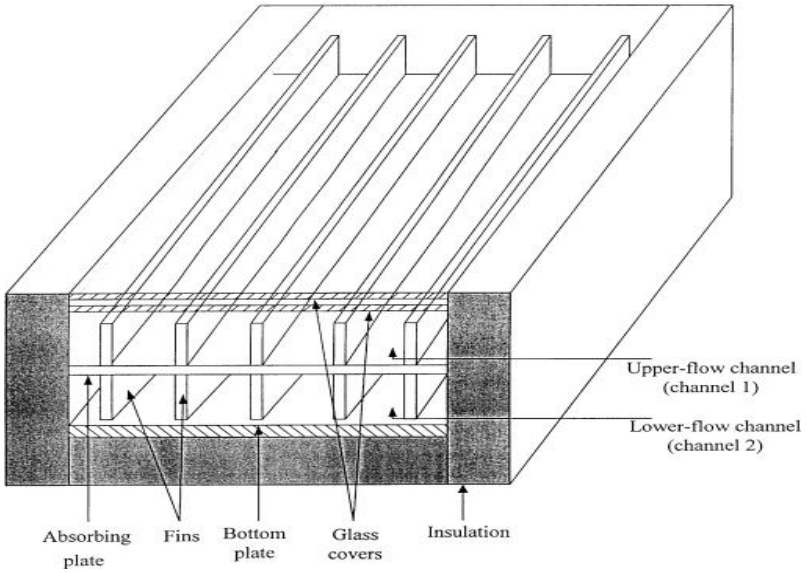

Figure 3.16 Double-flow solar air heater with fins attached

Paisarn Naphon [24] studied in detail about porous and non-porous media used in solar air heater. For describing the heat transfer characteristics of these arrangement they derived mathematical model by using energy conservation equations. They found that thermal conductivity of porous media affects the thermal performance of air heater. Around 25.9% higher efficiency they found for air heater which having porous media as compare to non-porous air heater. Schematic diagram of air heater with porous media and non-porous media is shown in “Figure 27” and “Figure 28” respectively.

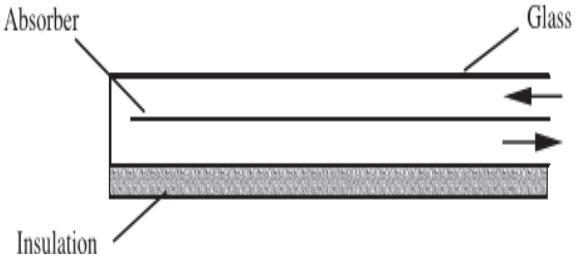

Figure 3.17 Schematic diagram of double pass solar air heater with porous media.

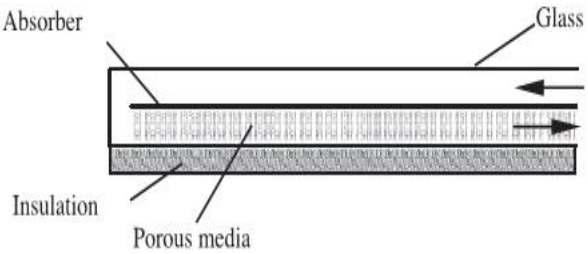

Figure 3.18 Schematic diagram of double pass solar air heater with porous media.

Filiz Ozgen et al. [13] investigated experimentally investigated the performance of double pass flat-plate collector having absorber plate, which is roughened by aluminum cans. They found that to improve the efficiency of air heater, it can be done by increasing the fluid velocity or by enhancing the heat transfer coefficient between fluid and absorber plate. Absorber plate were made by using aluminum materials at a suitable cost. Three different types of absorber plates designed by them. In first type (Type I) cans arranged in zigzag manner on absorber plate, while in Type II cans were arranged in order. Type III was smooth plate. They obtained highest efficiency for Type I at 0.05 kg/s of mass flow rate.

Figure 3.19 Absorber plate with Al cans arranged in transverse manner (Type II)

Figure 3.20 Absorber plate with Al cans arranged in transverse manner (Type I)

A.A. El-Sebaii et al. [1] theoretically as well experimentally studied the performance of double pass-finned solar air heater. Theoretically predicted value and experimentally calculated value gave fairly good agreement. They also compared the output power, outlet temperature and temperature of

absorber plate of double pass finned solar air heater which have V-corrugated plate. Result obtained by them are as follows:

1. DPVCPSAH (double pass V-corrugated plate solar air heater) is 9.3-11% more efficient than DPFIPSAH (double pass finned plate solar air heater).
2. Thermal efficiency of DPFIPSAH and DPVCPSAH up to a mass flow rate of 0.04 kg/s.
3. The maximum thermohydraulic efficiency for DPVCPSAH was found 17.4% more than DPFIPSAH.

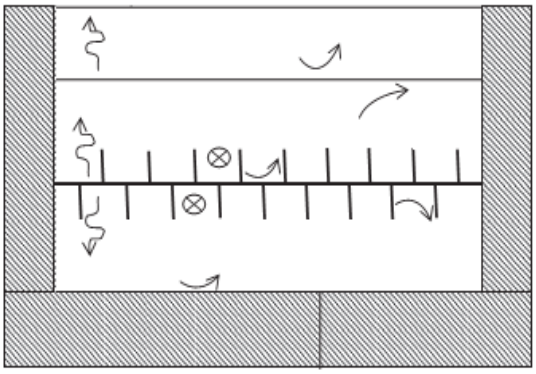

Figure 3.21 Double pass-finned solar air heater (DPFIPSAH)

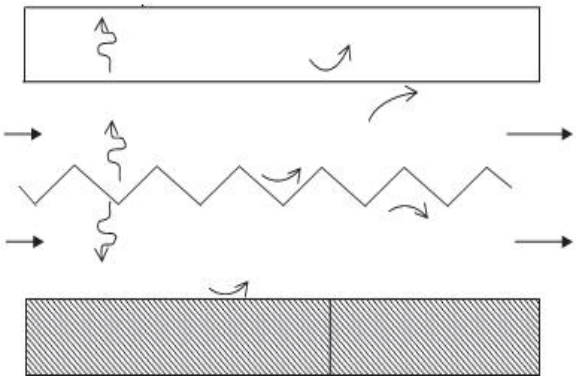

Figure 3.22 Double pass v-corrugated plate solar air heater (DPVCPSAH).

M.R.I. Ramadan et al. [21] investigated experimentally as well as theoritically the characteristics of packed bed double pass solar air heater. Limestone and gravel were used as material for packed bed. The effects of porosity of packed bed material and mass flow rate on thermal performance of air heater also disscused. They observed that high mass flow rate and low porosity of packed bed causes higher heat transfer rate. Thermohydraulic efficiency increases, with increase in mass flow rate of air upto 0.05 kg/s, beyond this an insignificant change occurs. Thermohydraulic efficiency was found to be maximum at 0.05 kg/s of mass flow rate. Gravel material gives better performance than lime-stone.

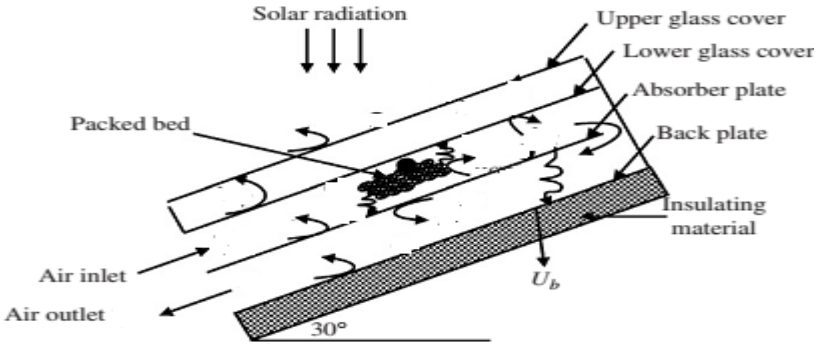

Figure 3.23 Double pass packed bed solar air heater.

M.F.El Khwajah et al. [20] studied the performance characteristics of fins attached on double pass solar air heater. Instead of an absorber plate between the fins wire mesh layer were used. Mass flow rate ranges from 0.0121-0.042 kg/s. They observed for same mass flow rate maximum efficiency was obtained by using 6 fins. For the mass flow rate of 0.042 kg/s the maximum efficiency obtained for 2, 4, 6 fins solar air heater were 75%, 82.1% and 85.9% respectively. Maximum average temparature difference between the inlet and outlet of air was found maximum for 6 fins solar air heater.

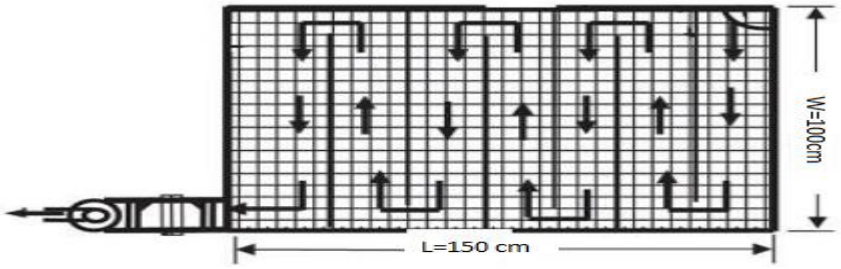

Figure 3.24 Fin attached double pass solar air heater having wire mesh as absorber.

Sunil Chamoli et al. [34] presented the review for analysis of performance of double pass solar air heater. The concept of making solar air heater with double pass involved of doubling the heat transfer area in cheaper cost. The main conclusion drawn by them as follows:

1. They found for DPSAH, many reaserchs had been done on porus media and extended surface, few researchs carried out on corrugated surface and no one reported for artificial roughned absorber plate on both sides.
2. It was observed if in both upper and lower channel mass flow rate and channel depths are same, than the maximum efficiency occurs.
3. By energy conservation analysis mathematical model prepared for solar air heater.

Dharam Singh et al. [12] presented a review for heat transfer enhancement by using artificial roughness on absorber plate of solar air heater. They observed it is best method to improve the efficiency of solar air heater by attaching the roughness element on absorber plate at cost of low to moderate power penalty for friction. It is the best passive technique to enhance the rate of heat transfer to fluid flow. They presented the effect of V corrugated ribs, transverse ribs, inclined ribs and discrete ribs on performance characteristics of solar air heater. They found that this methods improves the thermal performance of solar air heater.

Sudhanshu Dogra et al. [31] studied the characteristics of transverse and inclined ribs attached on absorbing plate of double pass solar air heater. Rectangular duct of aspect ratio (W/H) 10 was used.

Reynolds number varies from 4900-12000, p/e ratio ranges from5-20 for fixed value of e/D_h ratio as 0.044 and angle of attack (α) as 90°. They observed that maximum enhancement in heat transfer and friction factor occurs at relative roughness pitch (p/e) of 10 and maximum enhancement in heat transfer was 1.6 times more as compare to smooth plate due to occurrence of maximum reattachment point at this p/e ratio.

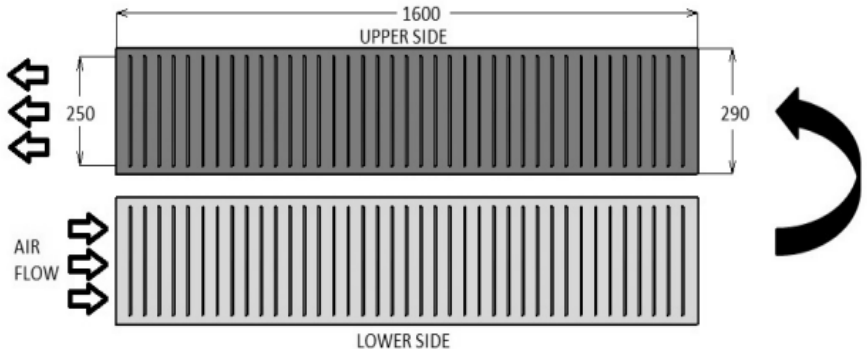

Figure 3.25 Schematic view of absorber plate attached with transverse ribs.

Avdhesh Sharma et al. [5] investigated the characteristics of V-shaped artificial ribs in double pass solar air heater. Roughness ribs attached on both sides of absorber plate in the form of V-shaped. The operating and roughness parameters were used for experiment as p/e ranges from 5-20, angle of attack (α) ranges from 30°-90°, Reynolds number ranges from 4900-15000 and e/D_h varies from 0.022-0.033. They observed that by providing artificial roughness on absorber plate of double pass solar air heater, in comparison to the smooth absorber plate heat transfer and friction factor both enhanced considerably for roughened absorber plate. On the basis of experimental calculated data they found that maximum enhancement in heat transfer and friction factor occurs at p/e ratio of 10, angle of attack (α) of 60° and e/D_h ratio of 0.033. Maximum heat transfer was 1.7 times of smooth plate and maximum friction factor was 1.9 times more than smooth plate found by them.

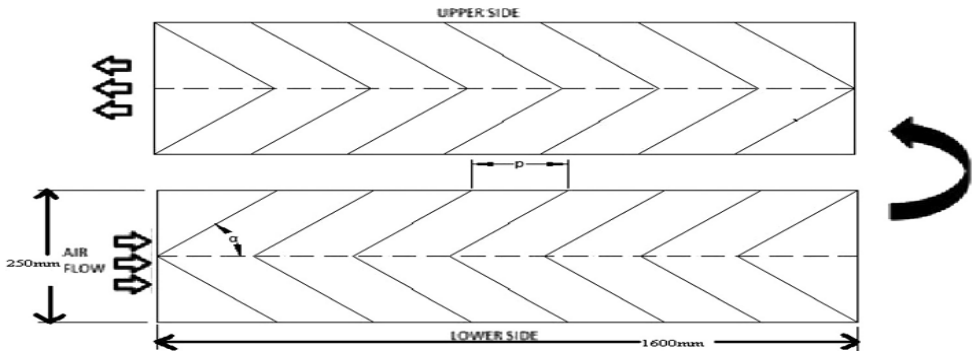

Figure 3.26 Schematic view of absorber plate artificially roughened with V-shaped ribs.

CHAPTER 4 RATIONALE AND SCOPE OF THE STUDY

4.1 Rationale of the Study

Solar air heaters are simple in design and easy to construct. Solar air heater are broadly used as collection devices and can be used in many applications such as space heating, crop drying, seasoning of timber, curing of industrial products etc. Due to low convective heat transfer coefficient between absorber plate and flowing air the efficiency of flat plate solar air heater is low, it increases the temperature of absorber plate, and this leads to higher heat losses from device to environment. There are some parameters on which performance of solar air heater depends as follows:

4.1.1 Solar Air Heater Performance Dependence Parameter

1. Rate of incident solar radiation.
2. Properties of absorber plate.
3. Types of solar air heater used.
4. Rate of convective heat transfer between air and absorber plate.
5. Losses from absorber plate.

We are not able to control the rate of incident solar radiation because it is natural process. Other parameter are more important which decides the specification and performance of solar air heater. There are some specific techniques which can be used for enhancement of the heat transfer to air by absorber plate in solar air heater.

4.2 Scope of the Study

How to enhance the performance of solar air heater? Solution of this question is main scope of the present study. Identify the different techniques for enhancement of thermal performance of solar air heater and choose best suitable method, which will leads to creation of most efficient solar air heater. There are some methods discussed below for enhancing the performance of air heater.

4.2.1 Minimize the Heat Losses

Heat loss is one of the main reason which results in lower heat transfer which further accounts for lower efficiency of the heater. So there is a need to minimize this heat loss so as to increase the properties of solar heater. Some of the ways of reducing heat losses from the solar collector are given below

1. By lowering convective as well as radiative heat losses.
2. By using vacuum or other medium in gap space.
3. By selective absorber surfaces.

4.2.2 Heat Transfer Improvement Techniques

The heat transfer coefficient is low between the absorber plate and the air flowing in the duct. This leads to high temperature of absorber plate and higher heat losses. The heat losses can be reduced by increasing the heat transfer coefficient or by reducing the absorber plate temperature. This can be achieved by following methods

4.2.2.1. By providing packed bed absorbers for solar air heating collectors

Solar radiation absorbs by the packed bed absorber in depth. It has high heat transfer capacity and high heat transfer area to volume ratio. So that the temperature of absorber plate will lower. This methods leads to increase in efficiency of the solar air collector. Efficiency increases up to 50% at low mass flow rate of fluid. The major disadvantage of this type of collector includes the high initial cost and large pumping power requirement as compared to conventional solar air heaters.

4.2.2.2 By using extended surface to increase area of heat transfer

Surfaces which are used to increase the area of heat transfer are called as extended surfaces i.e. fins. Bevill and Brandt [7] described that solar air collector which consist of parallel and uniformly spread out Al fins positioned below the cover plate of glass. The collector was designed to obtain high collector efficiency, with low pumping power to pass air through the collector. The result shows that by using superior fins the efficiency about 18% more could be obtained.

4.2.2.3 By using artificial roughness

For obtaining high convective heat transfer coefficient, it is necessary that flow above heat transfer surface should be turbulent. However blower and fan gives energy for generating turbulence. So extreme turbulence leads for extreme power requirement.

Therefore it is necessary for less power requirement turbulence should be created in laminar sublayer which is very near to the absorber surface. The heat exchange takes place in this region. To avoid excessive losses flow should not excessively disturbed. By using roughened on air side this can be achieved. Use of artificial roughness seems to be an attractive proposition for improving the coefficient of heat transfer.

By using any one technique from discussed above all techniques, leads in enhancement of performance of solar air heater. To choose best suitable method which will give best performance of solar air heater with less power penalty is the main objective of present study. The scope of present study encompassed in search of best suitable method for performance enhancement of solar air heater with less power penalty.

CHAPTER 5 OBJECTIVES OF THE STUDY

Following conclusion can be drawn from the literature survey

Solar air heater is renewable energy source device which converts the solar energy into heat energy. The heat transfer coefficient is low between air and absorbing plate of air heater, which leads in low efficiency. Low efficiency is the main problem in using solar air heater. To enhance the efficiency of solar air heater many researchers put their views. Some of these techniques are as follows

1. By using roughness element on absorber plate.
2. By use of extended surface i.e. fins.
3. By electro hydrodynamic method.
4. By providing packed bed.
5. By providing porous media.

Out of these methods simplest and most suitable method to increase the heat transfer is by using artificial roughness in different orientation on absorber plate. Few studies were carried out on double pass solar air heater having artificially roughened absorber plate.

5.1 Objectives of the Present Study

1. Study of a roughness geometry provided on absorber plate of solar air heater. Identification of new roughness geometry for absorber plate, i.e. W-shaped geometry.
2. Analysis the characteristics of W-shaped artificial roughness in double pass solar air heater.
3. Carry out the experimental investigation performance of a roughened solar air heater based on thermal efficiency, thermo-hydraulic efficiency, for different values of Reynolds number, for a selected W-shaped artificial roughness geometry.
4. Investigate the heat transfer appearances through rectangular duct of double pass solar air heater. Power penalty investigation for increase in friction factor.
5. Investigate and study the effect of roughness and flow parameter on thermal characteristics of solar air heater. The flow and roughness parameter are as follows
   - Reynolds Number (Re).
   - Relative roughness height (e/D_h).
   - Relative roughness pitch (p/e).
   - Angle of attack (α)
6. Develop the regression model to find the correlations for Nusselt number and friction factor.

CHAPTER 6 EXPERIMENTAL INVESTIGATION

6.1 Overview

From the literature review as discussed in chapter 3, all the studies revels that solar air heater having artificial roughened absorber plate more efficient as compare to smooth one. Creation of artificial roughness on absorber plate enhance the heat transfer as well as friction factor. Artificial roughness can be created by using ribs, by machining or by inserted tapes etc. Many investigators found that attaching ribs with glue is one of the effective method to produce artificial roughness on the absorber plate of a single pass solar air heater. The ribs are attached to the absorber plate in different orientation like transverse geometry, V-shaped, inclined, transverse etc. Many research's had been carried out to show the effect of artificial roughness on thermal performance of single pass solar air heater.

The main aim of the present study is to investigate the effect of W-shaped artificial roughness on thermal performance and friction characteristics of double pass solar air heater.

6.2 Experimental Apparatus

The schematic view of the experimental apparatus is shown in "Figure 6.1". The experimental apparatus consist of a double pass rectangular channel, plenum, solar simulator, pressure measuring devices, temperature measuring devices, and blower. A double pass rectangular channel has been designed and fabricated to study the effect of artificial roughness used in absorber plate of double pass solar air heater.

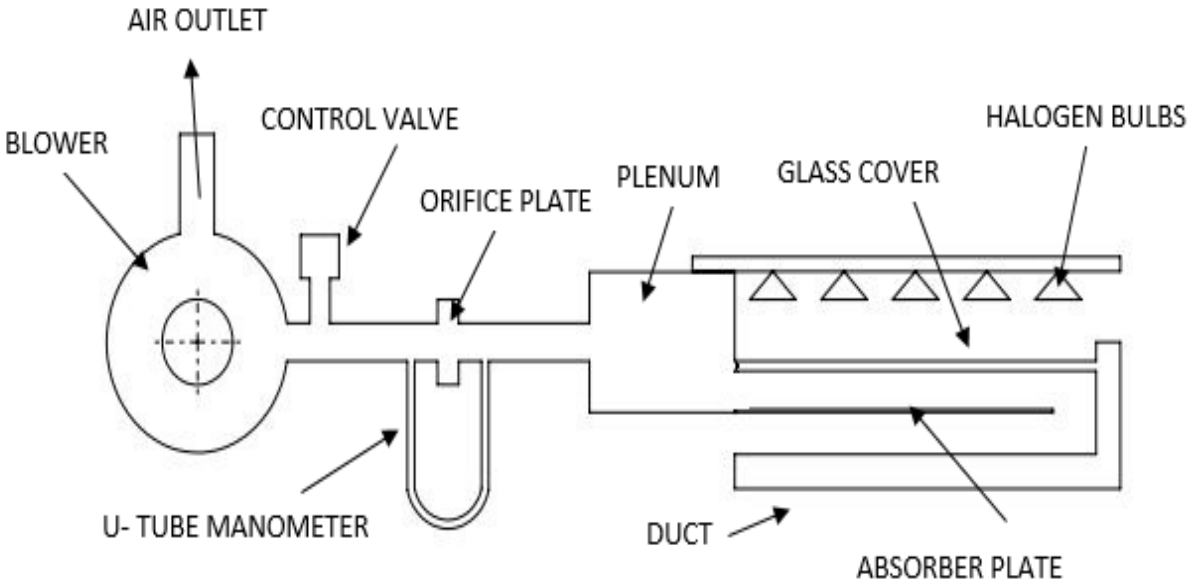

Figure 6.1 The schematic view of experimental apparatus.

The experimental apparatus consists of a rectangular channel which has been designed and fabricated from wood. The dimensions of the rectangular channel are 2070 mm × 250 mm × 25 mm. 50 mm is the total height of the rectangular channel as it is the case of double pass. The channel consists of entry section, test section and a small gap so that air can easily move up. The entry section has been designed according to ASHARAE standards [4] i.e. $5\sqrt{WH}$. Test section is of 1600 mm and 70 mm of gap is provided after test section for the proper circulation of air.

The atmospheric air is sucked through the lower channels suction blower having capacity of 3 HP through the lower portion of the double pass rectangular channel. The air moves to the upper portion of the rectangular channel through the gap present after the test section. The exit section of the channel is connected to a GI pipe via rectangular mixing chamber called plenum. Calibrated orifice plate provided in the GI pipe is used for measuring the mass flow rate of the air through duct. U-tube manometer and micro-manometer are used for measuring the pressure drop across the orifice plate and test section respectively.

The test section is of galvanized iron which acts as an absorber plate. The ribs attached on upper and lower portion of the absorber plate to make it roughened absorber plate. For providing constant heat flux to the absorber plate, a solar simulator is used. The temperatures of the heated absorber plate and air are measured by using 10k-ohm NTC thermistor and a digital micro-voltmeter. Two control valves are provided to control the mass flow rate of the air at the exit and entrance of the blower. The full description of the major components of the experimental set-up is given below

6.2.1 Duct of Solar Air Heater

The 3-D view of the duct is shown in "Figure 6.2". The duct is fabricated from the wooden plank of rectangular cross section. The dimension of the duct is 2070 mm × 250 mm × 25 mm and the aspect ratio (W/H) of the duct is 10. The length of the test section is 1600 mm. The duct is designed as per ASHARE standard [4]. The length of the entry section is given by$5\sqrt{WH}$.

The bottom of the duct has been made from 19 mm thick wooden plank with 6 mm thick plywood fixed on it and the other two sides has been made from 25 mm thick wooden plank. 1 mm thick sun mica laminate has been pasted on top of the ply wood in order to give good smooth surfaces. A gap of 70 mm is provided after the length of 2000 mm for the proper circulation of the air. A glass of thickness 4 mm is placed at a height of 50 mm so that double pass channel can be formed and solar radiation can be easily fall on the absorber plate. "Figure 6.3" and "Figure 6.4" shows the pictorial and sectional view of the duct respectively.

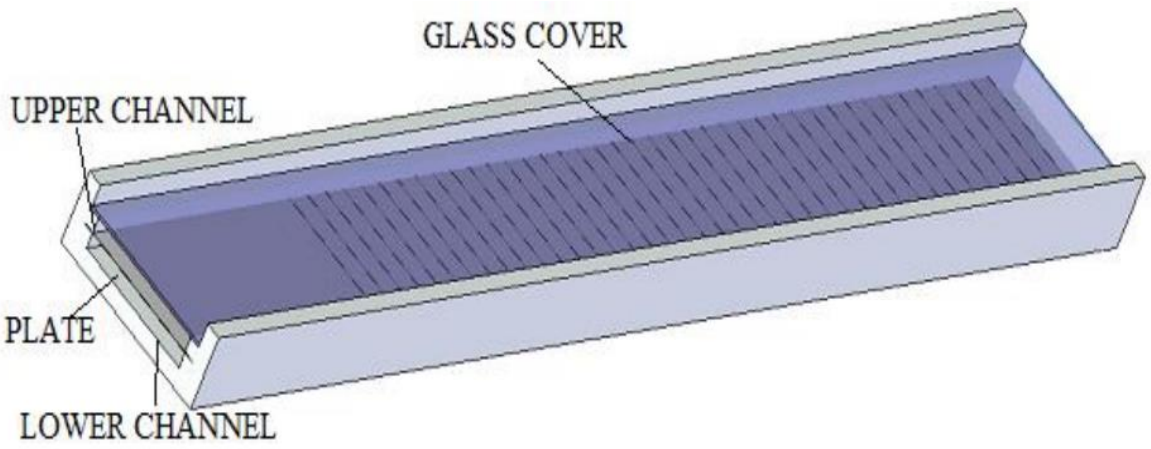

Figure 6.2 3-D view of Double pass solar air heater duct

Figure 6.3 Pictorial view of rectangular duct

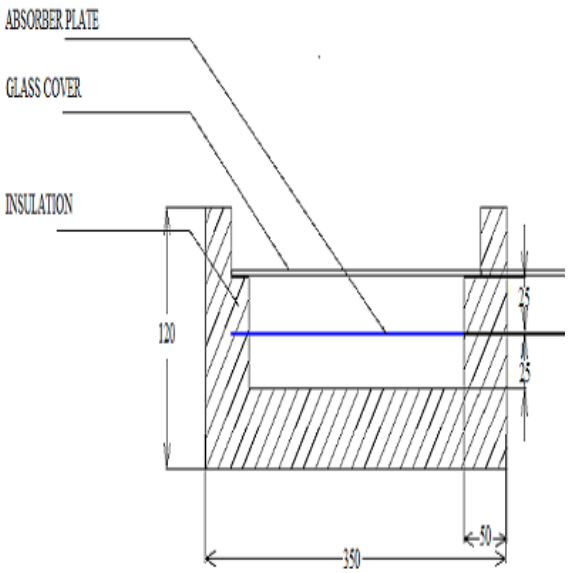

Figure 6.4 Sectional view of duct

6.2.2 Solar Simulator

Solar simulators have been design for both the non-concentrating and concentrating solar applications. The main objective of a solar simulator is to simulate the spatial and spectral distribution of solar radiations into a focal plane of a highly concentrating solar system. Schematic and Pictorial view of the solar simulator is given in "Figure 6.5" and "Figure 6.6" respectively. A solar simulator has been fabricated so that solar radiation of constant heat flux (900 W/m^2) can be fall on the absorber plate. It consists of six halogen lights of 500 watt each. These halogen light have been fixed on a stand in such a way that the radiations from the halogen light directly falls on the absorber plate. The heat flux of the radiation falling on the absorber plate through the halogen light is checked by pyrometer.

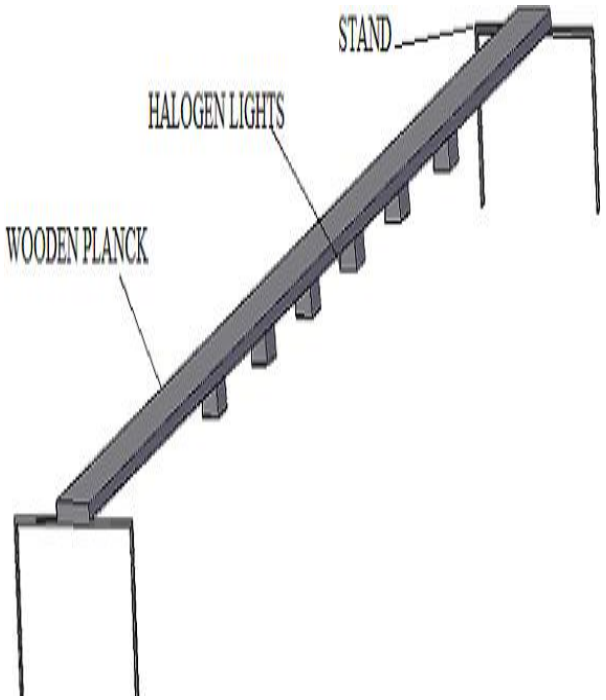

Figure 6.5 Schematic view of solar simulator

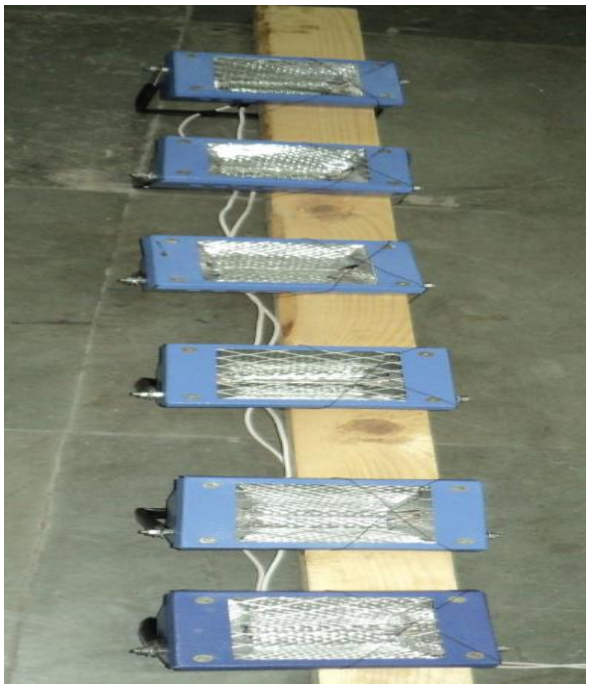

Figure 6.6 Pictorial view of solar simulator

6.2.3 Roughened Absorber Plate

A galvanized iron sheet has been used as an absorber plate. The size of the galvanized iron absorber plate is 1600 mm × 250 mm. artificial roughness in the form W-shaped has been provided on both side of the absorber plate. The absorber plate was heated from the topside by the help of the solar simulator and thus subjected to uniform heat flux. The schematic and pictorial view of roughened absorber plate with W-shaped ribs is shown in “Figure 6.7” and “Figure 6.8” respectively.

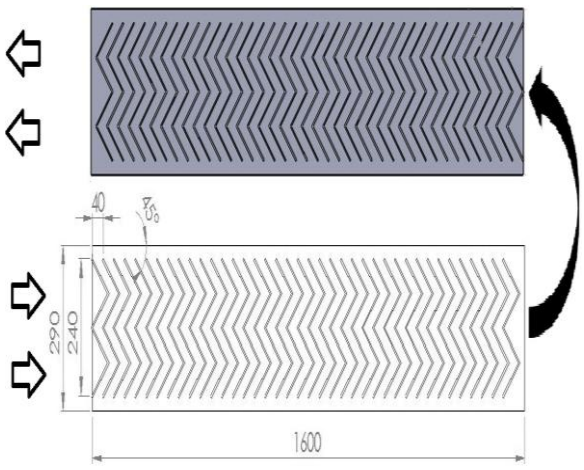

Figure 6.7 Cad model of roughened absorber plate.

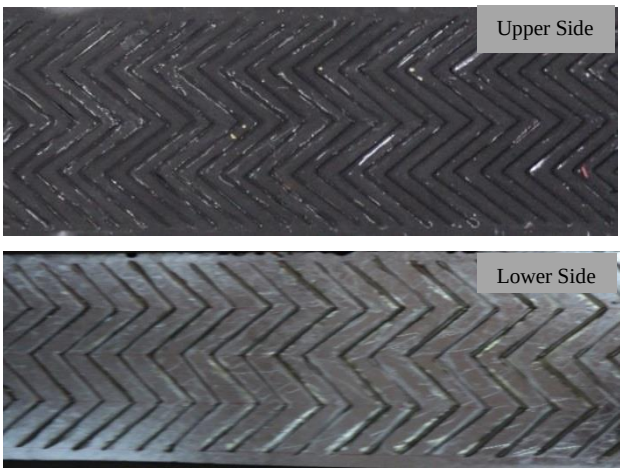

Figure 6.8 Artificial roughened plate with W-shaped (α=45°, p/e=20, e/Dh=0.044)

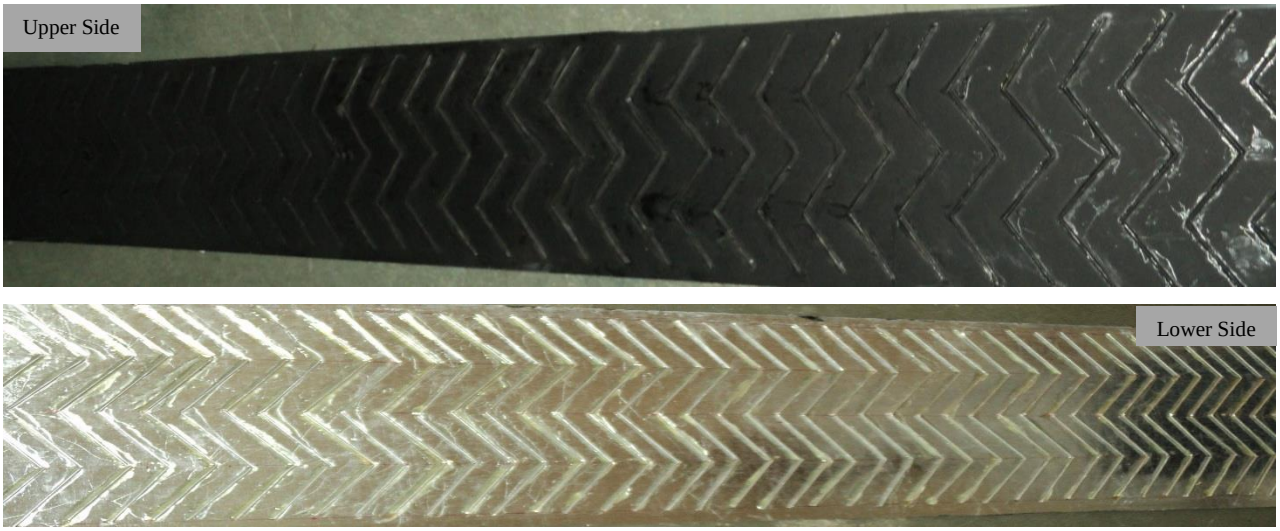

Figure 6.9 W-shaped roughened absorber plate at inclination angel (α) of 60°

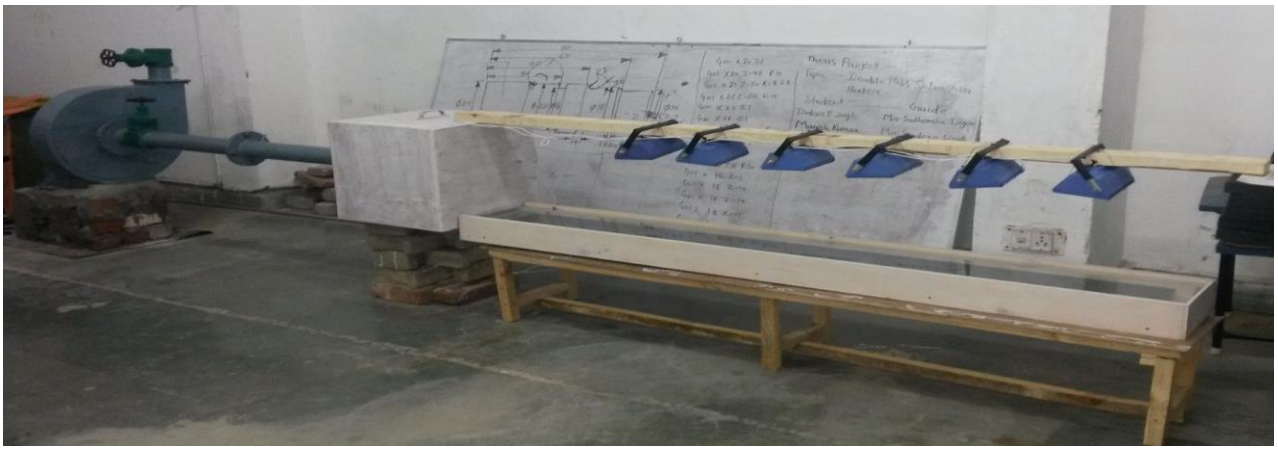

Figure 6.10 Pictorial view of experimental apparatus.

Figure 6.11 Experimental apparatus in running mode.

6.2.4 Air Handling Equipment (blower)

The centrifugal blower used for sucking ambient air through duct, which is driven by 3 HP, three phase, 290 V and 2900 rpm motor. The exit of the duct is connected to the blower by means of an 80 mm diameter galvanized iron pipe provided with a calibrated orifice plate and a plenum. Two valves are provided at the entrance and exit of the blower for the accurate control of the mass flow rate of air. The orifice plate assembly and the control valves are connected through a flexible plastic pipe of 600 mm length in order to minimize the transmission of vibrations from blower to the rectangular duct. All connecting parts are joined with gaskets and seals to prevent air leakages.

6.3 Instrumentation

6.3.1 Pressure Measurement

For measuring the pressure difference across test section a projection manometer is used. Least count of manometer is 0.01 mm. It consists of mainly 3 parts movable reservoir, fixed reservoir and transparent tube. These two reservoir connected with air inlet & outlet ports of duct through flexible tubes. By moving the reservoir up and down the meniscus is kept at fixed prescribed mark, the movement of reservoir noted down which yields the pressure drop across test section.

6.3.2 Temperature Measurement

Temperature of the air and the absorber plate were measured by using the 10k-ohm NTC thermistor. At the top of the absorber plate twelve thermistors were mounted and the temperature shown by them is then averaged to find the mean temperature of the absorber plate. Location of the thermistors is shown in "Figure 6.10". 2 thermistors provided at inlet and outlet of the te and then the temperature indicated by them were averaged to find out the mean temperature of air flowing through the duct for the estimation of different properties of air.

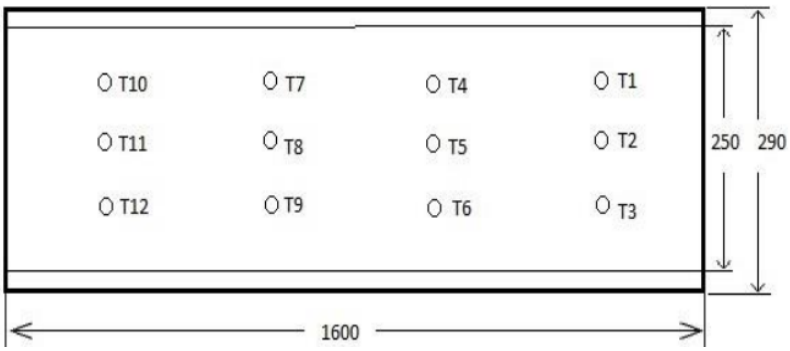

Figure 6.12 Location of the thermocouples on the absorber plate

6.3.3 Air Flow Measurement

The concentric orifice plate was used to measure the mass flow rate of air through duct. The orifice plate fitted in 80 mm GI pipe, which carrying the air from plenum to blower. The value of coefficient of discharge (C_d) was 0.612 and it is used to measure mass flow rate of the air. A U-Tube manometer has been used to measure the pressure drop across the orifice plate.

6.4 Roughness Geometry and Range of Parameters

The circular ribs are attached to the absorber plate with the help of glue in the form W-shaped. The main roughness geometry parameters are relative roughness pitch (p/e), relative roughness height (e/D_h) and angle of attack (α). Height and pitch of the ribs expressed by relative roughness height and relative roughness pitch respectively. Angle of attack (α) shows inclination of the ribs. The range of parameters is given in "Table 6.1"

Table 6.1 Range of roughness geometry and flow parameters

S. No.	Roughness geometry & flow parameter	Range
1.	Aspect Ratio of duct (W/H)	10
2.	Relative roughness pitch (p/e)	5-20
3.	Relative roughness height (e/D_h)	0.044
4.	Angle of attack (α)	45°-75°
5.	Reynolds number (Re)	6900-14000

6.5 Experimental Procedure

It is necessary to check all the joints of duct, pipe fittings, and inlet-outlet section of the duct for leakage. It is necessary condition for starting the experiment there should be no leakage of air. Pipe fittings, inlet-outlet section of duct, valves opening should be sealed properly in order to reduce the possibility of leakage.

Before collecting the data the set was allowed to attain quasi-steady state. The relevant data for temperatures were recorded at different mass flow rate of air under quasi-steady process. Then heat transfer, friction factor, thermal and thermohydraulic efficiency were calculated by using these collected data. After achieving the steady state condition the following data were recorded for calculation work

1. Absorber plate temperature at 12 different locations of absorber plate.
2. Temperature of air at inlet and outlet of the duct.
3. Reading of micro manometer for measuring pressure drop across test section
4. Measurement of pressure across orifice meter for finding mass flow rate of air through duct.

These raw data is used in data reduction and for further calculation work.

6.6 Data Reduction

The average air temperature, average plate temperature, Reynolds number and mass flow rate were calculated by using collected experimental data. Then these data were used to find the Nusselt number, friction factor and heat transfer coefficient. Thermal and thermohydraulic efficiency were also calculated by using these data. Relevant expressions for the computation of above mentioned parameters and some intermediate parameters have been given in "Table 6.2".

Table 6.2 Data reduction formulae

Parameters	Explanation	Formulae Used
Mean plate Temperature (T_p)	It is calculated by taking average of temperatures recorded at 12 different locations of absorber plate.	$T_P = \frac{T_1+T_2+T_3+\cdots+T_{12}}{12}$ (6.1)
Air Temperature (T_f)	Bulk mean temperature of air is mean of air temperature at inlet and outlet of test section.	$T_f = \frac{T_I+T_e}{2}$ (6.2)
Mass Flow Rate of Air (m)	Mass flow rate of air is calculated by measured pressure drop across the orifice meter.	$m=C_d A_0 \sqrt{\frac{2\rho\Delta P_0}{1-\beta^4}}$ (6.3)
Velocity of air through duct (V)	The velocity of air is calculated by mass flow rate and area of flow (area of duct).	$V = \frac{m}{\rho WH}$ (6.4)
Hydraulic Diameter (D_h)	It is calculated by using area of cross section and perimeter.	$D_h = \frac{4A_C}{P}$ (6.5)
Reynolds Number (Re)	The Reynolds number of airflow is calculated by knowing velocity, density, hydraulic diameter of duct and viscosity.	$Re = \frac{\rho V D_h}{\mu}$ (6.6)

Friction factor (f)	Darcy Wiesbach equation is using to calculate friction factor by measuring pressure drop across test section.	$f = \frac{2(\Delta P)D_h}{4\rho LV^2}$ (6.7)
Heat transfer rate (Q_u)	Heat transfer rate (Qu) to the air is calculated by using inlet and outlet temperature of air.	$Q_u = mC_p(T_o - T_i)$ (6.8)
Heat transfer coefficient (h)	The heat transfer coefficient (h) is calculated by knowing the plate temperature and area of heating surface.	$h = \frac{Q_u}{A_p(T_p - T_f)}$ (6.9)
Nusselt Number (Nu)	Nu is calculated by using h, D_h and conductivity of air.	$Nu = \frac{hD_h}{k}$ (6.10)

6.7 Validation of Experimental Apparatus

The experimental setup must be validated before collecting the experimental data. In order to validate the experimental setup an experiment carried out on smooth plate. Nusselt number and friction factor calculated by using the collected experimental data. Then these experimental data have been compared with predicted value, which is calculated from Dittus-Boelter equation [26] and Modified Blasius equation [18]. "Figure 6.11" and "Figure 6.12" shows that the comparison of experimental value and actual value (predicted value) of the Nusselt number and friction factor respectively. Dittus-Boelter equation and modified Blasius equation are as follows

Dittus-Boelter equation:

$$Nu_s = 2 \times 0.024 Re^{0.8} Pr^{0.4} \quad (6.11)$$

Modified Blasius equation:

$$f_s = 2 \times 0.085 Re^{-0.25} \quad (6.12)$$

This is the case of double pass solar air heater so that the value of Dittus–Boelter equation and Modified Blasius equation are two times of the original value. Equation 6.11 and equation 6.12 are Dittus-Boelter equation and Modified Blasius equation respectively. The validity curves are shown below which shows the comparison of actual value (calculated from eq. 6.11 &6.12) and experimentally calculated value of Nusselt number and friction factor. Then after comparison following results are obtained.

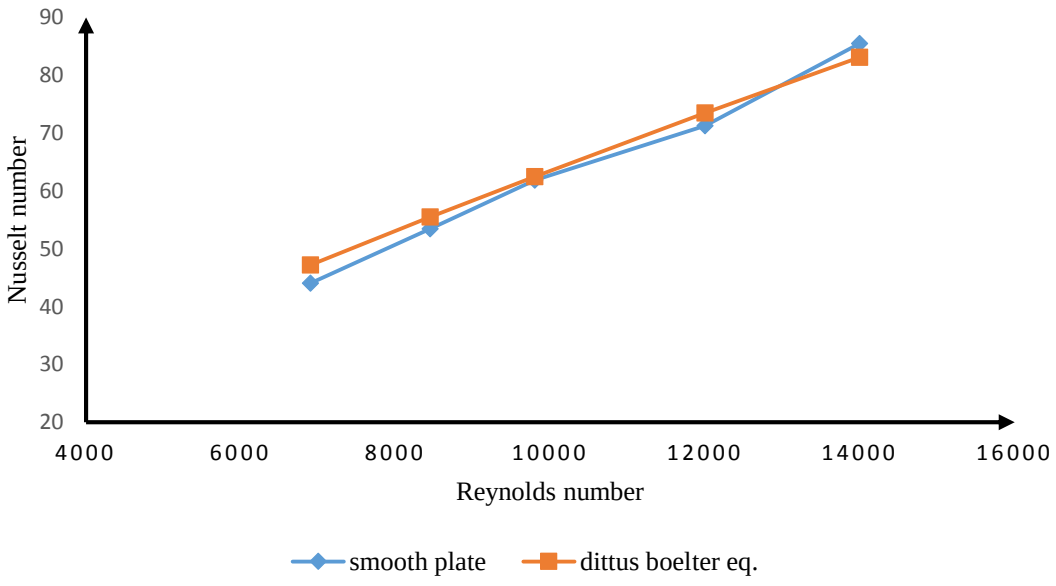

Figure 6.13 Validity curve between experimental value and predicted value of Nusselt number for smooth plate.

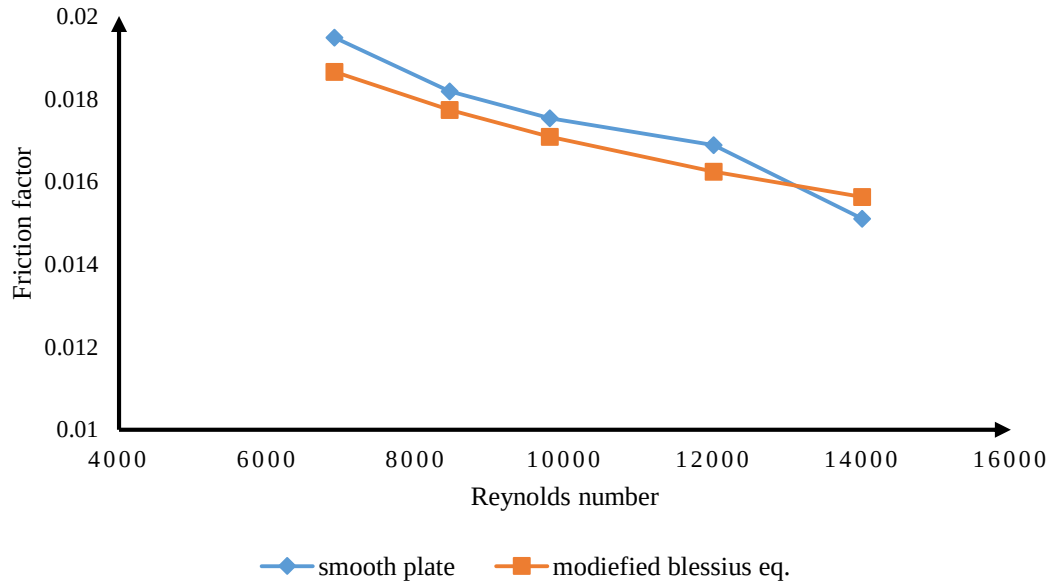

Figure 6.14 Validity curve between experimental value and predicted value of friction factor for smooth plate.

The maximum deviation in the predicted and experimental value of Nusselt number and Friction factor is found to be 5.2% and 3.1% respectively. This gives confidence in experimental data obtained from the set up and its instruments.

CHAPTER 7 RESULTS AND DISCUSSION

7.1 Overview

Roughness element is present in both sides of the absorber plate, due to this roughness geometry flow become turbulent when it is come in contact with roughened absorber plate. The main reasons for turbulent flow over roughened absorber plate are separation of flow, due to destroy of laminar sub layer or due to formation of reattachment point at the periphery absorber plate. Maximum heat transfer occurs at reattach point of flow. Due to use of roughness element on absorber plate, heat transfer coefficient increase but on the other hand, friction factor also increases which leads to increase in pumping power. In this chapter a discussion on how friction factor and heat transfer get affected by flow and roughness parameters. Roughness parameters are relative roughness height (e/Dh), inclination angle of ribs (α) and relative roughness pitch (p/e). Flow parameters are Reynolds number (Re) and mass flow rate of air through duct. Then performance of roughened solar air heater has been compared with smooth one.

This chapter contains three sections. First section arguments about how the friction factor and Nusselt number are affected by roughness and flow parameters. In the next section correlations developed for Nusselt number and friction factor. In the last section thermal and thermohydraulic performance of solar air heater having artificial roughened absorber plate have been discussed.

7.2 Consequences of Roughness Parameters on Nusselt Number & Friction Factor

7.2.1 Consequence on Nusselt Number

The experimentally collected values of Nusselt number have been plotted against Reynolds number for different values of roughness parameter. The Nusselt number is governed by roughness parameter like inclination angle of ribs (α), relative roughness pitch (p/e), roughness height (e/Dh) and flow parameter like Reynolds number (Re). The ranges of parameters have been taken as discussed in chapter 6 (Table 6.1). Nusselt number is important parameter, which decides the behavior of heat transfer in solar air heater. The effect of various roughness and operating parameter on the heat transfer of double pass solar air heater is given below. Maximum heat transfer occurs at inclination angle of ribs (α) 60° and relative roughness pitch (p/e) of 10.

7.2.1.1 Consequence of Relative Roughness Pitch (p/e)

"Figure 7.1" shows the deviation in Nusselt number against Reynolds number. The inclination angle of ribs and relative roughness height (e/D_h) is fixed as 60° and 0.044 respectively. The relative roughness pitch (p/e) ranges from 5-20 for experiment. The graph shows how the Nusselt number is

affected by W-shaped ribs on absorber plate for variable values of Reynolds number and relative roughness pitch (p/e).

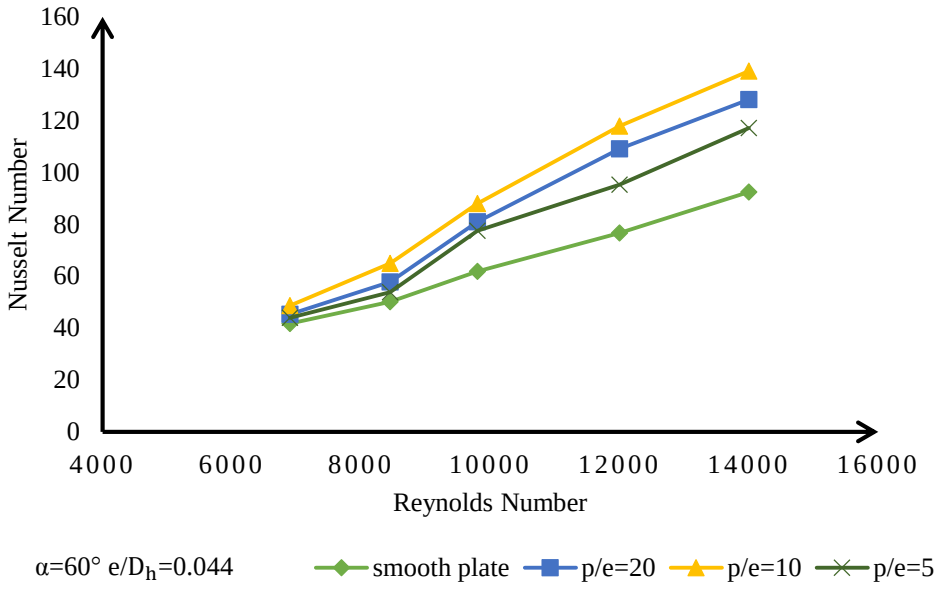

Figure 7.1 A plot of Nusselt number against Reynolds number for ranges of p/e ratio.

From "Figure 7.1" it is clear that Nusselt number increases continuously as Reynolds number increase. At fixed inclination angle of ribs (α) of 60^0, fixed relative roughness height of 0.044 and relative roughness pitch (p/e) of 10 the maximum Nusselt number occur. Maximum heat transfer occur at reattachment point hence, maximum heat transfer occur at this relative roughness pitch. Prasad and Saini [25] reported that reattachment points on the absorber surface starts decreasing when relative roughness pitch (p/e) goes on increasing. Heat transfer starts decreasing due to decrease in reattachment points. The flow gets separated while being downstream of a rib but does not get reattached if the relative roughness pitch (p/e) is less than 10 as in case of p/e ratio of 5. No reattachment of flow occurs at relative roughness pitch (p/e) less than 10. So optimum value of relative pitch (p/e) is 10 for maximum heat transfer.

"Figure 7.2" shows the how the Nusselt number varies with relative roughness pitch (p/e) for ranges of Reynolds number. Inclination angle of ribs (α) and relative roughness height (e/D_h) are fixed as 60° and 0.044 respectively. The significant variation has been seen in Nusselt number at higher Reynolds number but with decrease in Reynolds number the effect on Nusselt number become insignificant. These results shows the how much heat transfer is affected by orientation of the artificial ribs geometry.

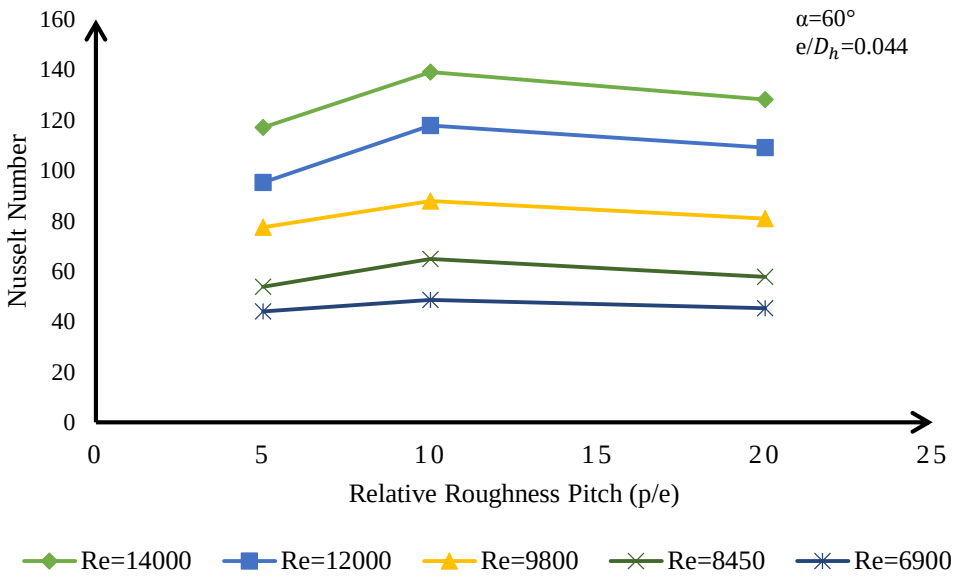

Figure 7.2 A plot of Nusselt number against p/e ratio for ranges of Reynolds number.

7.2.1.2 Consequence of inclination angle of ribs (α)

"Figure 7.3" shows effect of operating and roughness parameter on Nusselt number and heat transfer of double pass solar air heater. A graph has been plotted between friction factor and Reynolds number for different values of inclination angle of ribs (α). Inclination angle of ribs varies from 45°-75°. Relative roughness height (e/D_h) and Relative roughness pitch (p/e) are fixed as 0.044 and 10 respectively.

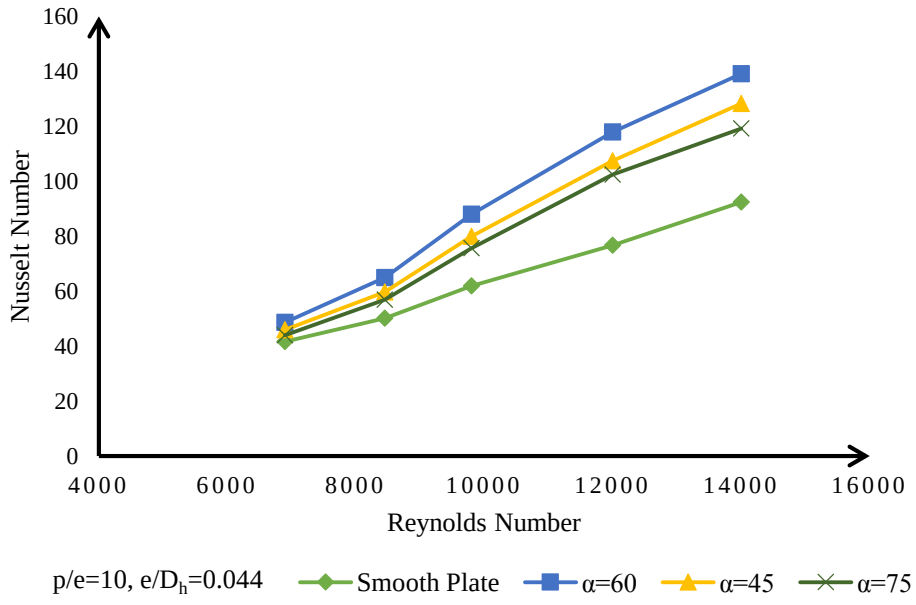

Figure 7.3 A plot of Nusselt number against Reynolds number for varying inclination angle (α).

The graphs shows that by increasing inclination angle of ribs (α), Nusselt number get increases. Hans et al. [16] studied the effect of providing angles to the on heat transfer and they reported that due to inclination of ribs with respect to flow, an anti-rotating secondary flow creates along span of ribs. This reason causes variation in heat transfer coefficient along the span of ribs. The anti-rotating secondary flow gets increases with increase in inclination of ribs up to a certain limit, further increase in ribs inclination results in decreased secondary flow. Due to this reason maximum heat transfer occurs at inclination angle of ribs (α) of 60°. At 45° and 75° inclination of ribs less heat transfer occur as compare to 60°. "Figure 7.4" shows the variation of Nusselt number as a function of inclination angle of ribs (α).

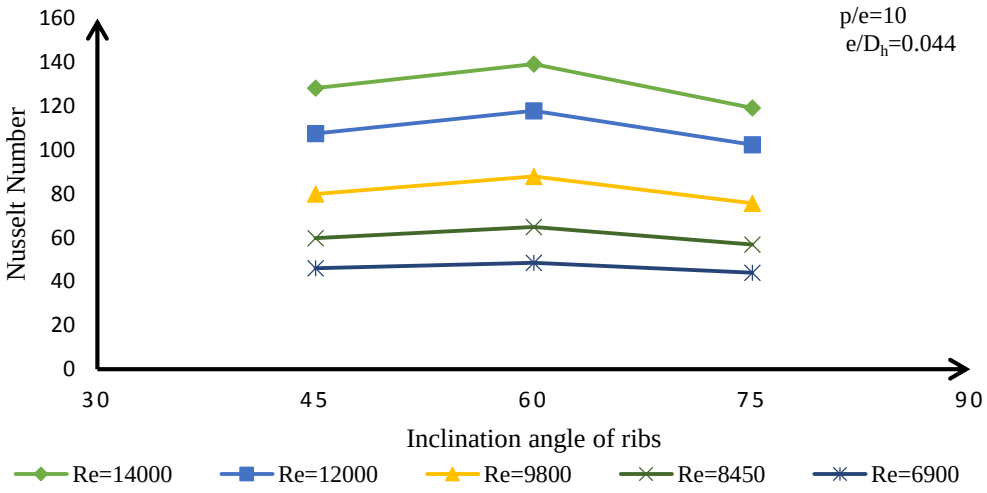

Figure 7.4 A plot of Nusselt number against inclination angle (α) for ranges of Reynolds number.

7.2.2 Consequence on Friction Factor

In this section effect of W-shaped artificial roughness on friction factor features have been discussed. For different roughness geometry parameters friction factor (f), which is obtained from experiments plotted as a function of Reynolds number. Same as Nusselt number, the friction factor is also governed by roughness parameter like inclination angle of ribs (α), relative roughness pitch (p/e), roughness height (e/D_h) and flow parameter like Reynolds number (Re). The ranges of roughness and flow parameters have been remain same as discussed in previous section. At inclination angle of ribs (α) of 60° and relative roughness pitch (p/e) of 10, the maximum friction factor occurs.

7.2.2.1 Consequence of Relative Roughness Pitch (p/e)

As discussed earlier friction characteristics of solar air heater is function of inclination angle of ribs (α), relative roughness pitch (p/e), relative roughness height (e/D_h) and Reynolds number (Re).

"Figure 7.5" shows the variation in friction factor as a function of Reynolds number. The inclination angle of ribs and relative roughness height (e/D_h) are fixed as 60° and 0.044 respectively. The relative roughness pitch (p/e) varies from 5 to 20 for experiment. It is found that with the increase in Reynolds number, the friction factor decreases for all values of p/e ratio. The maximum value of friction factor occurs at relative roughness pitch (p/e) of 10.

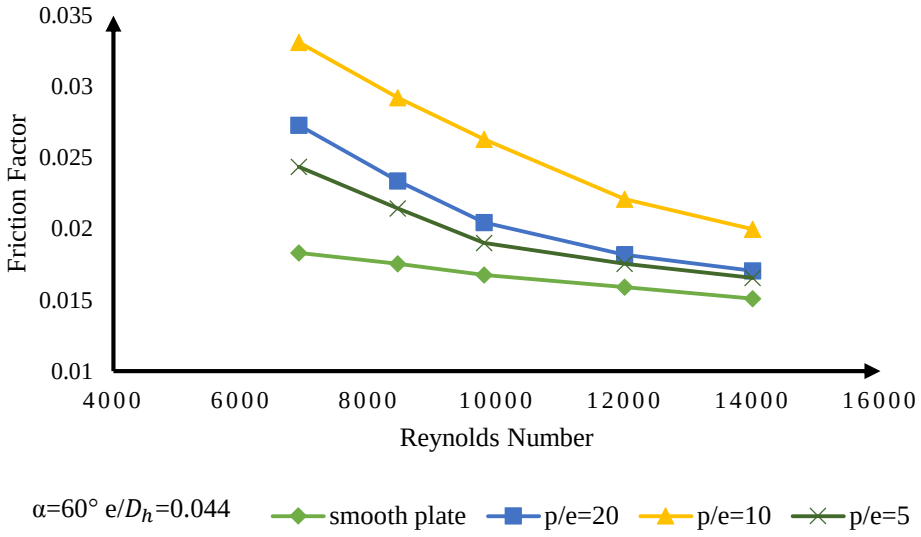

Figure 7.5 A plot of friction factor against Reynolds number for ranges of p/e ratio.

A graph has been plotted between friction factor and Reynolds number as shown in "Figure 7.5". The graph shows that friction factor linearly decreases with increase in Reynolds number for all values of relative roughness pitch (p/e).

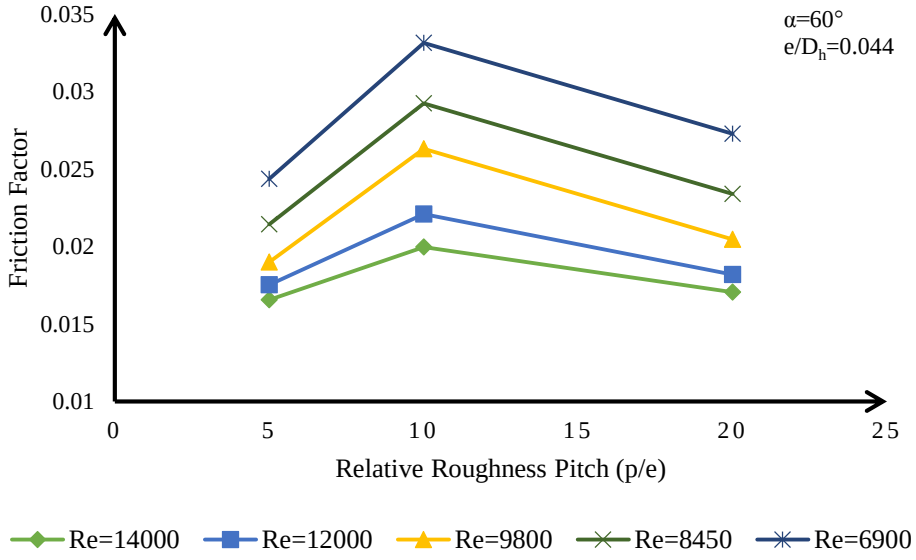

Figure 7.6 A plot of friction factor against p/e ratio for ranges of Reynolds number.

Maximum friction factor occurs at relative roughness pitch (p/e) of 10 for fixed inclination angle of ribs (α) of 60° and relative roughness height (e/D_h) of 0.044, as shown in "Figure 7.5". "Figure 7.6" shows the variation in friction factor as a function of relative roughness pitch (p/e) for ranges of Reynolds number. The result shows roughness parameter at which maximum heat transfer occur, friction factor also get maximum at that orientation of roughness element.

7.2.2.2 Consequence of inclination angle of ribs (α) on Friction Factor

A graph is plotted between the friction factor and Reynolds number for different values of inclination angle of ribs (α). The inclination angle of ribs (α) has been taken as 45°, 60° and 75°. The relative roughness pitch (p/e) and relative roughness height (e/D_h) fixed as 10 and 0.044 respectively.

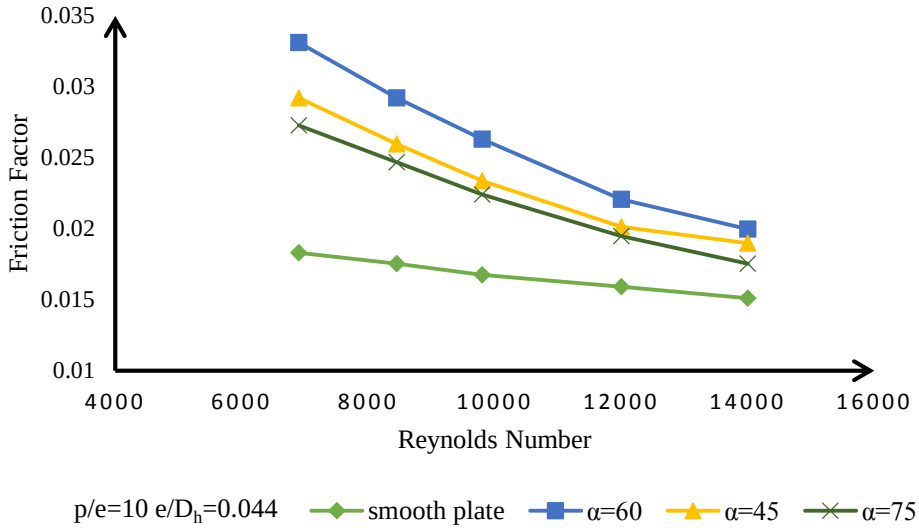

Figure 7.7 A plot of friction factor against Reynolds number for ranges of inclination angle (α).

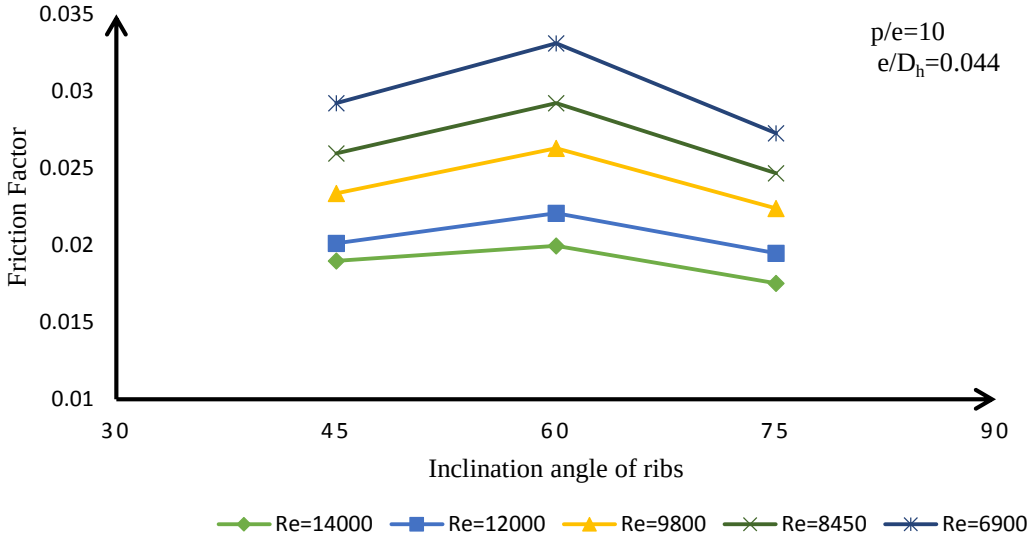

Figure 7.8 A plot of friction factor against inclination angle (α) for ranges of Reynolds number.

"Figure 7.7" shows the variation of friction factor as a function of Reynolds number for different inclination angle of ribs and fixed relative roughness pitch (p/e) and relative roughness height (e/D_h). It is observed that maximum friction factor occur at inclination angle of ribs (α) of 60°, because maximum anti rotating secondary occur at this inclination angle of ribs. The variation of friction factor with inclination angle of ribs for ranges of Reynolds number and fixed relative roughness pitch (p/e) and relative roughness height (e/D_h) has been plotted in "Figure 7.8".

7.3 Regression Model for Deriving Correlations

7.3.1 Overview

From the previous section, it is clear that Nusselt number and friction factor closely depends on the roughness parameter and flow parameter. The heat transfer increases in double pass solar air heater by creating artificial roughness on absorber plate. Power penalty also increases, due to increase in friction factor. The relationship of Nusselt number and friction with roughness and flow parameter can be expressed as:

$$Nu = Nu(Re, p/e, \propto, e/D_h) \quad (7.1)$$

$$f = f(Re, p/e, \propto, e/D_h) \quad (7.2)$$

Earlier S.K. Saini et al. [29] developed correlations for Nusselt number and friction factor for arc shaped wire shaped roughness element on absorber plate of solar air heater. They found maximum deviation in predicted values (calculated by correlation) and experimentally calculated values are ±10% for both Nusselt number and friction factor. Brij Bhushan et al. [8] developed correlations for protrusion roughness element and found deviation in predicted value (calculated by correlation) and experimentally calculated values are ±15% and ±10% for Nusselt number and friction factor respectively. The main aim of present study is development of correlations for Nusselt number and friction factor for double pass solar air heater having W-shaped artificial roughness ribs. Correlations have been developed for Nusselt number and friction factor by taking reference of Sanjay et al. [27].

7.3.2 Correlations for Nusselt Number

All the obtained values of Nusselt number from experimental data for different roughness geometry parameters have been plotted as a function of Reynolds number, as shown in "Figure 7.9".

Above graph shows that almost linear relationship between Nusselt number and Reynolds number. From regression analysis a straight line is fitted through these points and given as:

$$Nu = A_0 Re^{1.4405} \quad (7.3)$$

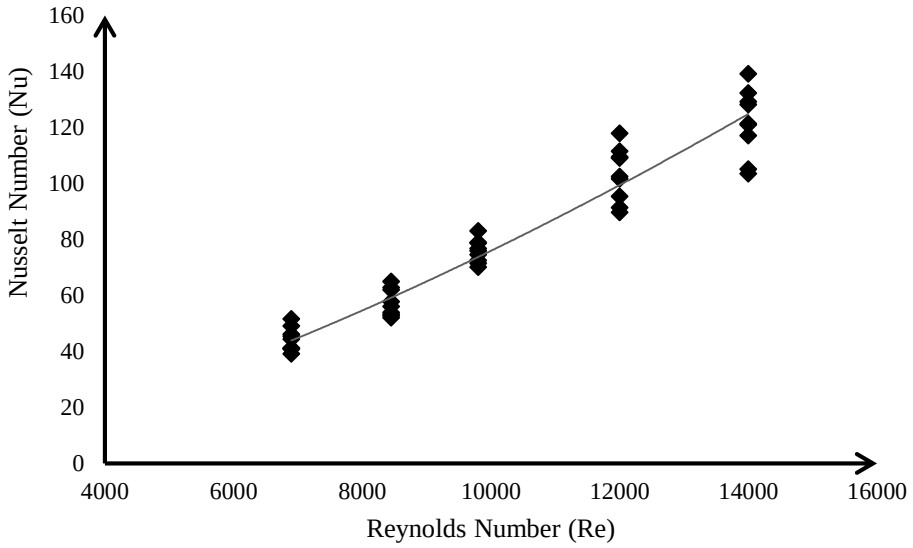

Figure 7.9 A plot between Nusselt number (Nu) and Reynolds number (Nu).

The coefficient of this equation A_0 is function of other influencing roughness parameter, i.e. relative roughness pitch (p/e). Now taking relative roughness pitch p/e as next consideration, and plot a graph between ($\frac{\mathrm{Nu}}{\mathrm{Re}^{1.4405}}$) and p/e on ln-ln scale as shown in "Figure 7.10".

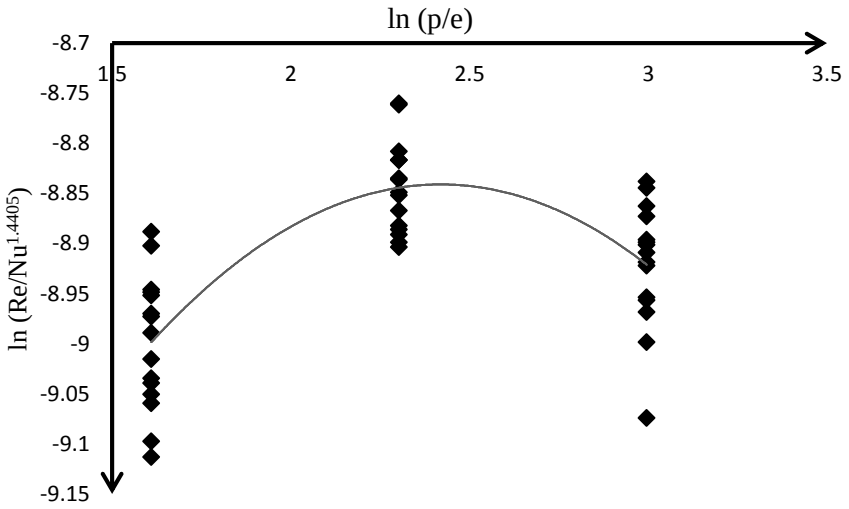

Figure 7.10 A plot between ln ($\frac{\mathrm{Nu}}{\mathrm{Re}^{1.4405}}$) and ln (p/e).

From second order polynomial regression following result obtained:

$$\ln\left(\frac{\mathrm{Nu}}{\mathrm{Re}^{1.4405}}\right) = \mathrm{B}_0 + 1.1626\ln\left(\mathrm{p}/\mathrm{e}\right) - 0.2403\left[\ln\left(\mathrm{p}/\mathrm{e}\right)\right]^2 \qquad (7.4)$$

This equation can be expressed as:

$$\frac{\mathrm{Nu}}{\mathrm{Re}^{1.4405}} = \mathrm{B}_0\left(\mathrm{p}/\mathrm{e}\right)^{1.1626} \times \exp[-0.2403\{\ln\left(\mathrm{p}/\mathrm{e}\right)\}^2] \tag{7.5}$$

Where, B_0 is the function of roughness parameter ($\frac{\alpha}{60}$). Value of B_0 plotted against ($\frac{\alpha}{60}$) as shown in "Figure 7.11".

$$B_0 = \frac{\mathrm{Nu}}{\mathrm{Re}^{1.4405} \times \left(\mathrm{p}/\mathrm{e}\right)^{1.1626} \times \exp[-0.2403\{\ln\left(\mathrm{p}/\mathrm{e}\right)\}^2]} \tag{7.6}$$

A regression analysis is implemented to fit a straight line through these points is expressed by:

$$\frac{\mathrm{Nu}}{\mathrm{Re}^{1.4405} \times \exp[-0.2403\{\ln\left(\mathrm{p}/\mathrm{e}\right)\}^2] \times \left(\mathrm{p}/\mathrm{e}\right)^{1.1626}} = \mathrm{C}_0\left(\frac{\propto}{60}\right)^{-0.035} \tag{7.7}$$

The values of coefficients are:

A_0 =0.0001, B_0 = -7.1264, C_0 =0.0008.

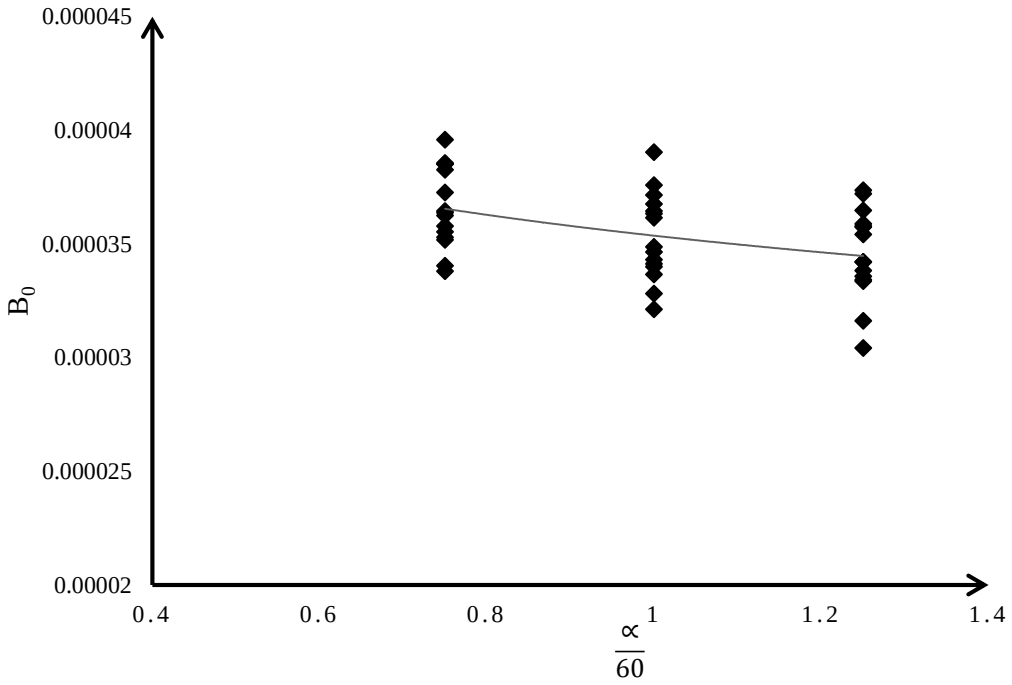

Figure 7.11 A plot between B_0 and $\frac{\propto}{60}$.

These values of the coefficients result in the following correlation for the Nusselt number:

$$Nu = 0.0004 \times Re^{1.4403} \times \exp\left[-0.2403\{\ln\left(\mathrm{p}/\mathrm{e}\right)\}^2\right] \times \left(\mathrm{p}/\mathrm{e}\right)^{1.1626} \times \left(\frac{\propto}{60}\right)^{-0.035} \tag{7.8}$$

7.3.3 Correlation for Friction Factor

All the obtained values of friction factor from experimental data for different roughness geometry parameters have been plotted as a function of Reynolds number, as shown in "Figure 7.12". Graph shows that almost linear relationship between friction factor and Reynolds number. From regression analysis a straight line is fitted through these points and given as:

$$f = D_0 Re^{-0.621} \tag{7.9}$$

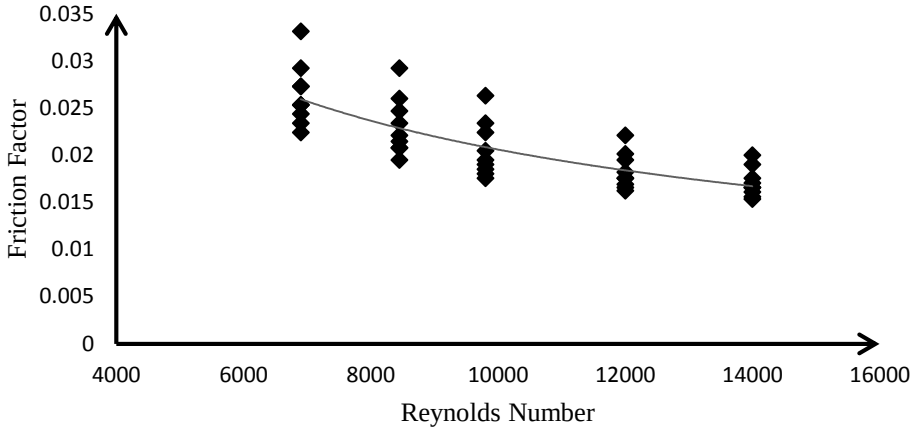

Figure 7.12 A plot between friction factor and Reynolds number.

The coefficient of this equation D_0 is function of other influencing roughness parameter, i.e. relative roughness pitch (p/e). Now taking relative roughness pitch p/e as next consideration, and plot a graph between ($\frac{f}{(Re)^{-0.621}}$) and (p/e) on ln-ln scale as shown in "Figure 7.13".

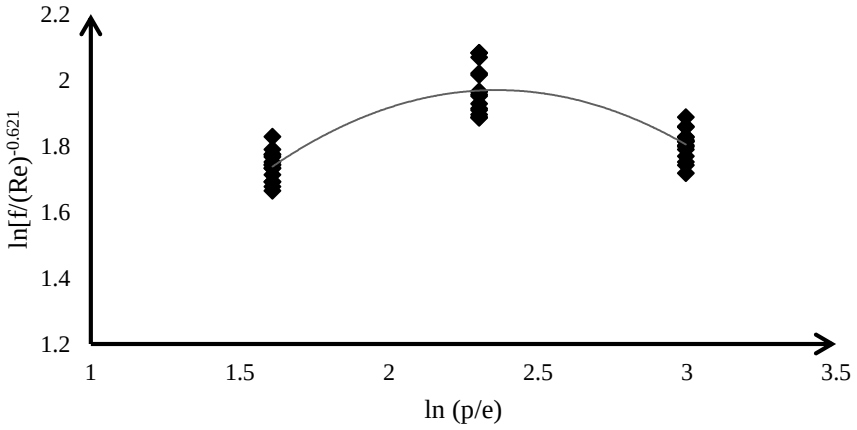

Figure 7.13 A plot between $\frac{f}{(Re)^{-0.621}}$ and ln (p/e).

From second order polynomial regression following result obtained:

$$\ln\left(\frac{f}{\mathrm{Re}^{-0.621}}\right) = \mathrm{E}_0 + 1.9352\ln\left(\mathrm{p}/\mathrm{e}\right) - 0.4098\left[\ln\left(\mathrm{p}/\mathrm{e}\right)\right]^2 \quad (7.10)$$

This equation can be expressed as:

$$\frac{\mathrm{f}}{\mathrm{Re}^{-0.621}} = \mathrm{E}_0\left(\mathrm{p}/\mathrm{e}\right)^{1.9352} \times \exp[-0.4098\left\{\ln\left(\mathrm{p}/\mathrm{e}\right)\right\}^2] \quad (7.11)$$

Where, E_0 is the function of roughness parameter ($\frac{\alpha}{60}$). Value of E_0 plotted against ($\frac{\alpha}{60}$) as shown in "Figure 7.14".

$$\mathrm{E}_0 = \frac{\mathrm{f}}{\mathrm{Re}^{-0.621} \times \left(\mathrm{p}/\mathrm{e}\right)^{1.9352} \times \exp[-0.4098\left\{\ln\left(\mathrm{p}/\mathrm{e}\right)\right\}^2]} \quad (7.12)$$

A regression analysis is implemented to fit a straight line through these points is expressed by:

$$\frac{\mathrm{f}}{\mathrm{Re}^{-0.621} \times \exp[-0.4098\left\{\ln\left(\mathrm{p}/\mathrm{e}\right)\right\}^2] \times \left(\mathrm{p}/\mathrm{e}\right)^{1.9352}} = \mathrm{F}_0\left(\frac{\propto}{60}\right)^2 \quad (7.13)$$

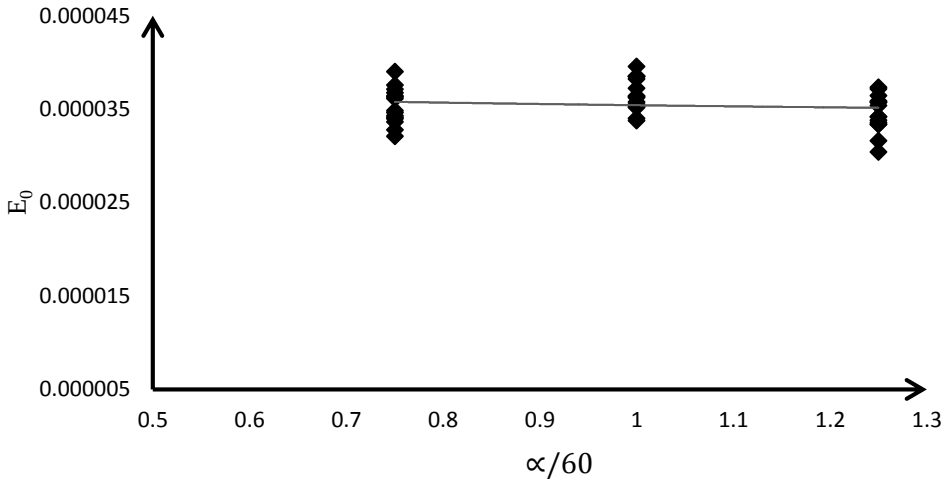

Figure 7.14 A plot between E_0 and$\frac{\propto}{60}$.

The values of coefficients are:

D_0 =6.287, E_0 = -0.3156, F_0 =0.7286.

These values of the coefficients result in the following correlation for the Nusselt number:

$$\mathrm{f} = 0.7268 \times \mathrm{Re}^{-0.621} \times \exp\left[-0.4098\left\{\ln\left(\mathrm{p}/\mathrm{e}\right)\right\}^2\right] \times \left(\mathrm{p}/\mathrm{e}\right)^{1.9352} \times \left(\frac{\propto}{60}\right)^{-0.067} \quad (7.14)$$

7.3.4 RESULTS

"Figure 7.15" and "Figure 7.16" shows the comparison of predicted value (calculated by correlation) and experimental value of the Nusselt number and friction factor respectively. "Figure 7.15" shows the deviation of ±11% between the experimental and predicted values of the Nusselt number which is in a fair acceptable limit. "Figure 7.16" shows the deviation of ±7% between the experimental and predicted values of friction factor which is also in good acceptable limit.

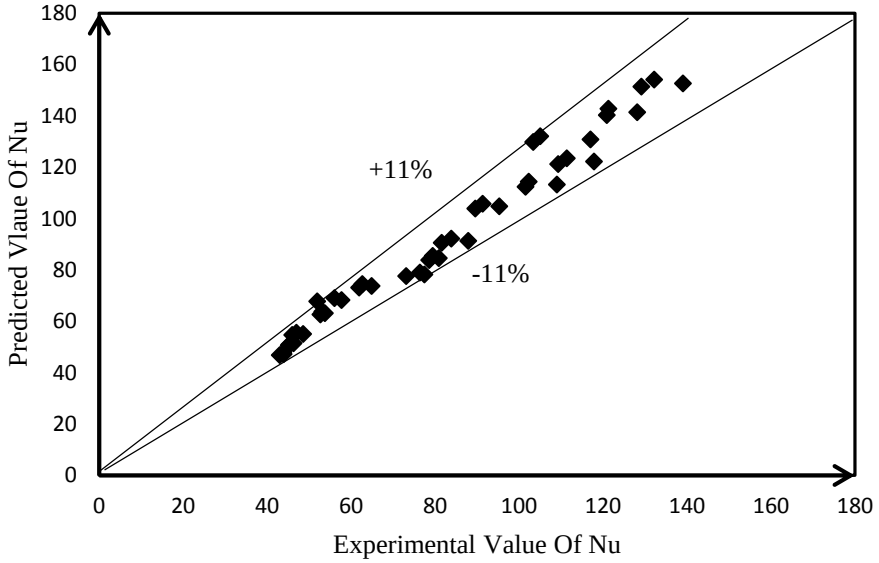

Figure 7.15 Comparison of experimental and predicted value of Nusselt number.

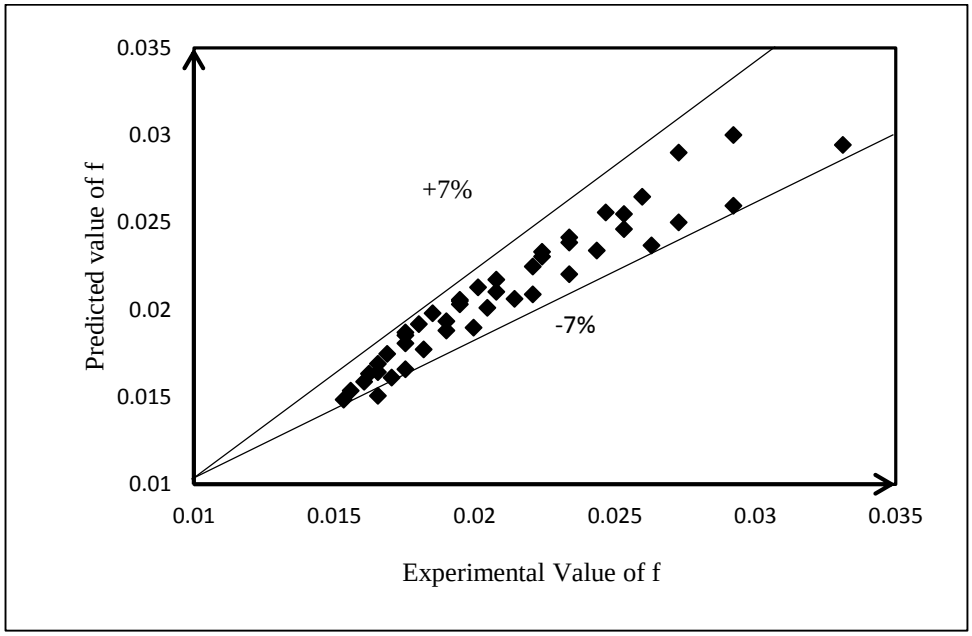

Figure 7.16 Comparison of experimental and predicted value of friction factor.

7.4 Thermal Performance

7.4.1 Overview

Solar energy used for many applications like solar cell, solar air collector and solar air heater as discussed earlier. It is generally termed as solar thermal energy, because in all such applications solar energy is converted into thermal energy. The efficiency of solar air heater is low due to low heat transfer coefficient between the flowing fluid and absorber plate. To enhance the efficiency of solar air heater many researcher have been given their idea, out of all those ideas increase the efficiency of solar air heater providing artificial roughness is the most common method which gets employed now a days. Till now single pass solar air heater have been mostly used, in which artificial roughness ribs are provided only in single side. In present study ribs are provided on both sides of the absorber plate to make it more efficient. This artificial roughness break the laminar sub layer and makes the flow turbulent adjacent to the absorber plate, which results in the increase in heat transfer. This chapter has been devoted to investigate the effect of W-shaped artificial roughness on thermal performance of double pass solar air heater. The effects of roughness and flow parameter on thermal performance have been discussed in this chapter. Enhancement in thermal efficiency of solar air heater by providing artificial roughness element, as compare to conventional smooth solar air heater also discussed.

7.4.2 Thermal Efficiency

7.4.2.1 Thermal efficiency evaluation procedure

The collected experimental data have been used to determine the value of thermal efficiency of the solar air heater having roughened and smooth absorber plates according to the following procedure:

Step I: Mass flow rate is calculated by using measured pressure drop across orifice plate, hence mass flow rate calculated by:

$$m = C_d A_0 \sqrt{\frac{2\rho \Delta P_o}{1-\beta^4}} \tag{7.15}$$

Step II: Heat gain by air is calculated by:

$$Q_u = mC_p(T_o - T_i) \tag{7.16}$$

Step III: Thermal efficiency is calculated by:

$$\eta_{th} = \frac{Q_u}{IA_p} \tag{7.17}$$

Where, I is the intensity of heat flux falling over absorber plate. A_p is the area of test section.

In the section effect of roughness and flow parameter on thermal efficiency of solar air heater have been discussed. Roughness and flow parameters remain same as discussed in previous chapter. Relative roughness height (e/D_h) is fixed of 0.044. Effect of relative roughness pitch (p/e) and inclination angle of ribs (α) on thermal efficiency have been discussed.

7.4.2.2 Consequence of Relative Roughness Pitch (p/e)

Figure 7.18 shows a plot in between thermal efficiency against Reynolds number for different relative roughness pitch (p/e). Inclination angle of ribs (α) and relative roughness height (e/D_h) are fixed as of 60° and 0.044 respectively. Variation in relative roughness pitch is from 5 to 20. Relative roughness pitch (p/e) varies from 5-20. The extreme thermal efficiency arises at inclination angle of ribs (α).

If relative roughness pitch surges past 10 then thermal efficiency starts falling, as flow separation occurs while being downstream of rib and does not get reattached. As the gap among the ribs are very minor at the relative roughness pitch of 5 it acts as a smooth plate thus thermal efficiency observed at this pitch is quite similar to that of a smooth plate, at this pitch due to minor gap among ribs doesn't cause any flow separation hence again there are no reattachment points formed. Hence highest intensity of heat transfer is observed at 10 relative roughness pitch.

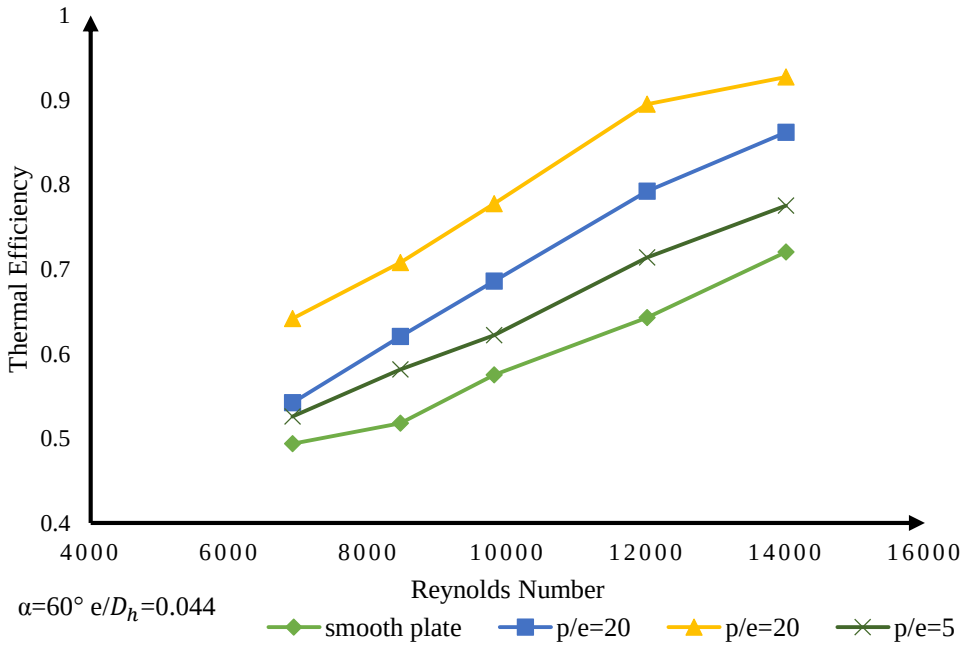

Figure 7.17 Variation of thermal efficiency as a function of Relative roughness pitch (p/e).

7.4.2.3 Effect of inclination angle of ribs (α)

In "figure 7.19" it has been shown that how thermal efficiency relies on Reynolds number. Inclination angle of ribs (α) is varies from 45° to 75° keeping relative roughness height (e/D_h) and relative roughness pitch (p/e) fixed as of 0.044 and 10 respectively. It has been observed maximum thermal efficiency occurs at Inclination angle of ribs (α) of 60°.

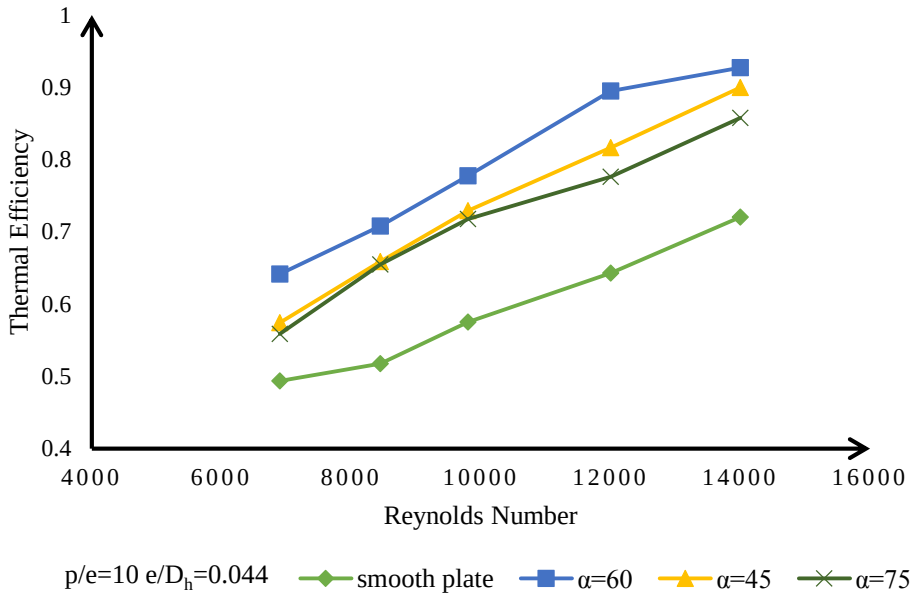

Figure 7.18 Variation of thermal efficiency as a function of Inclination angle (α).

Hans et al. [16] studied the effect of providing angles to the on heat transfer and they reported that an anti-rotating secondary flow creates along span of ribs due to inclination of ribs relative to flow. This reason causes variation in heat transfer coefficient along the span of ribs. The anti-rotating secondary flow gets increases with increase in inclination of ribs up to a certain limit, further increase in ribs inclination results in decreased secondary flow. Due to this reason peak heat transfer is observed at inclination angle of ribs (α) of 60°. At 45° & 75° inclination of ribs less heat transfer occur as compare to 60°.

7.5 Thermohydraulic Performance

7.5.1 Overview

As discussed in previous section flow should be turbulent over absorber plate. The turbulence is created with the help of the blower or fan & extreme turbulence means larger frictional losses and thus greater power is required. Turbulence is needed to be originated in a region adjacent to duct surface for keeping the frictional losses at minimum possible level.

The thermohydraulic efficiency of solar air heater is an effective efficiency, which is calculated by using actual thermal gain by air from absorber plate of solar air heater. In thermal efficiency we neglect the pumping power to run the blower for creating turbulence. For calculating thermohydraulic efficiency we also consider the pumping power required to generate turbulence.

7.5.2 Thermohydraulic efficiency

7.5.2.1 Thermohydraulic efficiency evaluation procedure

Thermohydraulic performance is the system's performance including characteristics of thermal and hydraulic behavior.

Thermohydraulic performance = Thermal performance + Hydraulic characteristics

The pumping power must be taken into account during the performance evaluation of solar air heater. Losses are also significant fraction of the energy during its transmission & conversion. The effective efficiency is the real performance of the collector which accounts equivalent thermal energy and useful thermal gain which will be necessary in providing mechanical energy for incapacitating frictional power losses, and is given by:

$$\eta_{eth} = \frac{Q_u - \frac{P_m}{C}}{IA_p} \tag{7.18}$$

Where $C = \eta_F \eta_m \eta_{Th} \eta_{Tr}$ is conversion factor which represents net conversion efficiency of mechanical energy to thermal energy.

η_F = Fan or blower efficiency.

η_m = Electrical motor efficiency used for driving fan.

η_{Th} = Electrical transmission efficiency.

η_{Tr} = Power plant's thermal conversion efficiency.

By calculations value of C is comes out to be 0.2.

Heat gain by the air is given by:

$$Q_u = mC_p(T_o - T_i)$$

The product of volume flow rate and the pressure drop ΔP_d through the duct is the mechanical power (P_m) which is required to flow the air through solar air heater. This power (P_m) is given by:

$$P_m = A \times V \times \Delta P_d \tag{7.19}$$

Where, pressure drop across the duct is given by micro manometer.

Based on a method as proposed by Cortes and Piacentini [11] the effective efficiency of roughened as well as smooth absorber plate solar air heater is calculated. The effects of various roughness parameters on thermohydraulic efficiency as follows:

7.5.2.2 Effect of relative roughness pitch (p/e)

The variation of thermohydraulic efficiency as a function of Reynolds number keeping inclination angle of ribs (α) and relative roughness height (e/D_h) are fixed as of 60° and 0.044 respectively has been shown in "Figure 7.19". Relative roughness pitch (p/e) varied from 5 to 20. The peak value of thermal efficiency is observed at relative roughness pitch (p/e) of 10.

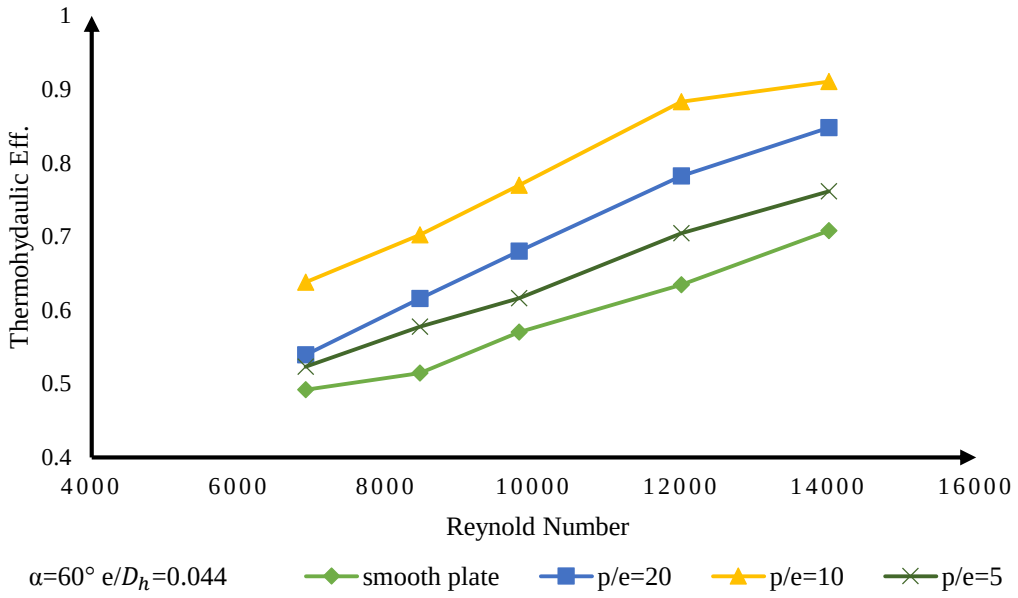

Figure 7.19 Variation of thermohydraulic efficiency as a function of Relative roughness pitch.

7.5.2.3 Effect of inclination angle of ribs (α)

The variation of thermohydraulic efficiency with respect to Reynolds number is shown in "Figure 7.20". Inclination angle of ribs (α) varies from 45° to 75° keeping relative roughness height (e/D_h) and Relative roughness pitch (p/e) fixed as of 0.044 and 10 respectively. It has been observed maximum thermal efficiency occurs at Inclination angle of ribs (α) of 60°.

Thus, it is clear from the plot above that the thermal and thermo hydraulic efficiency of a double pass solar air heater is maximum in case of α=60° with relative roughness pitch (p/e=10), because at p/e=5 the roughened plate generally behaves like a smooth plate. The ribs attached are very close to each other hence no vortex regions formed. Both thermal and thermohydraulic

efficiency of solar air heater having roughened absorber plate with W-shaped ribs is more as compare to smooth one.

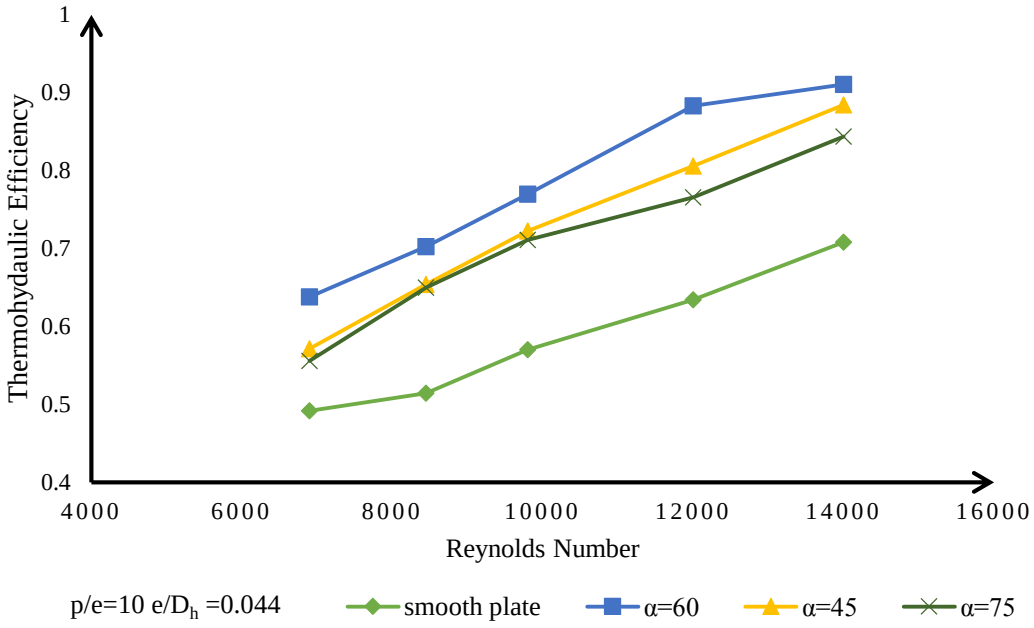

Figure 7.20 Variation of thermohydraulic efficiency as a function of inclination angle (α).

CHAPTER 8 CONCLUSION AND FUTURE SCOPE

The present study is based on an experimental investigation for evaluating the effects of W-shaped artificial roughness ribs on characteristics like heat transfer, thermal performance and friction factor on a double pass solar air heater. These ribs are attached both sides of the absorber plate in the form of W-shaped. A discussion on how the roughness & flow parameter will affect heat transfer and friction factor have been discussed.

Thermal and thermohydraulic performance of double pass solar air heater is also discussed in present study. For double pass solar air heater friction factor correlations and Nusselt number correlations have been developed. Based on experimental investigation following conclusions have been drawn.

8.1 Conclusions

The following conclusions have been drawn from this experimental investigation:

1. By enabling rectangular double pass solar air heat with W-shaped artificial roughness on both sides of absorber plate both friction factor and heat transfer is enhanced.
2. The maximum enhancement in heat transfer for roughened solar air have been observed 1.70 times of smooth one for fixed value of relative roughness height (e/D_h) of 0.044 at inclination angle of ribs (α) of 60°and relative roughness pitch (p/e) of 10.
3. Maximum friction factor occur at for fixed value of relative roughness height (e/D_h) of 0.044 at inclination angle of ribs (α) of 60°and relative roughness pitch (p/e) of 10. Maximum enhancement in friction factor for roughened solar air heater has been observed 1.81 times of smooth one.
4. For double pass solar air heater friction factor correlations and Nusselt number correlations have been developed on various roughness and flow parameters. The peak deviation between predicted value (calculated by correlation) and experimentally calculated value of Nusselt number and friction factor was found to be ±11% and ±7% respectively.
5. The maximum improvement in thermal and thermohydraulic efficiency for W-shaped artificially roughened solar air heater have been found around 20-21% more than the conventional smooth solar air heater. Maximum efficiency occur at fixed value of relative roughness height (e/D_h) of 0.044 at inclination angle of ribs (α) of 60°and relative roughness pitch (p/e) of 10.

8.2 Future Scope

1. The present study can be carried out for mathematical modelling.
2. A detailed experimental study for double pass solar air heater having discrete W-shaped ribs.

3. The different new geometries can be searched in future and can be compared with present study for heat transfer and friction characteristics.
4. To obtain best geometry for different range of roughness and flow parameter, an optimization study can be carried out.
5. There is a lot of scope of Flow visualizations over selected roughness geometry by using the flow visualization technique.
6. For forecasting optimized roughness element parameters Computational Fluid Dynamics (CFD) based models can be analysed for the study of flow characteristics and heat transfer of artificially roughened solar air heater.

REFERENCES

[1] A.A. El-Sebaii, S. A.-E. Thermal performance investigation of double pass-finned plate solar air heater. Applied Energy 88 , (2011) 1737-1739.

[2] Abdul-Malik Ebrahim Momin a, J. S.. Heat transfer and friction in solar air heater duct with V-shaped rib roughness on absorber plate. International Journal of Heat and Mass Transfer 45, (2002) 3383-3396.

[3] Anil Singh Yadav, J. L. Heat transfer and fluid flow analysis of an artificially roughened solar air heater a CFD based investigation. Front. Energy, (2014), 1-11.

[4] ASHARAE Standard. Method of testing to determine the thermal performance of Solar air heater. New York, (1997), ASHARAE Standard.

[5] Avdhesh Sharma, V. P. Heat transfer and friction characteristics of double pass solar air heater having V-shaped roughness on the absorber plate. Journal of Renewable and Sustainable Energy 5, (2013), 103-109.

[7] Bevill, V.D. and Brandt, H. A solar energy collector for heating air, Solar Energy 12, (1968), 19-29.

[8] Brij Bhushan, Ranjit Singh. Nusselt number and friction factor correlations for solar air heater duct having artificially roughened absorber plate. Solar Energy 85, (2011), 1109–1118.

[9] Bhagoria, J. S. Heat trasnsfer coefficient and friction factor correlation for rectangular solar air heater duct having transverse wedge shape rib roughness on the . Renewable energy 25, (2002) 341-369.

[10] C. Chaudhary, P.M. Chauhan. Performance and cost analysis of two-pass solar air heaters. Heat Recovery Systems & CHP Vol. No.8, (1995), 755-773.

[11] Cortes, A. and Piacentini, R., Improvement of the efficiency of a bare solar collector by means of turbulent promoters, Applied Energy 36 (1990), 253-261.

[12] Dharam Singh, V. Heat Transfer Enhancement of Solar Air Heater By Using Artificial Roughness–Review. International Journal of Engineering Trends and Technology 4, (2013), 4434-4436.

[13] Filiz Ozgen, Mehmat Esen. Experimental investigation of thermal performance of a double-flow solar air heater having aluminum cans. Renewable Energy 34 (2009) 2391–2398.

[14] Gaurav Bhardwaj, M. K.. Effect of inclined continuous ribs as roughness element on the absorber plate. International Journal of Sustainable Energy, (2012) 1-16.

[15] G. D. Rai. Non-Conventional energy sources. New Delhi: Khanna Publication, (2011).

[16] Hans, V.S., Saini, R.P. and Saini, J.S., Performance of artificially roughened solar air heaters – A review, Renewable and Sustainable Energy Reviews 13 (2010), 1854-1869.

[17] H.M.Yeh, C. D. Ho. Collector efficiency of double-flow solar air heaters with fins attached, Energy 27, (2002), 715–727.

[18] Kays W.M., P. H.. Handbook of Heat transfer. New York: Tata McGraw-Hill, (1973).

[19] Lanjewar, A. B.. Experimental study of augmented heat transfer and friction in solar air heater with different orientations of W- rib roughness. Experimental Thermal and Fluid Science 35, (2011), 986-995.

[20] M.F. El-khawajah, L.B.Y. Aldabbagh. The effect of using transverse fins on a double pass flow solar air heater using wire mesh as an absorber. Solar Energy 85 (2011), 1479–1487.

[21] M.R.I. Ramadan, A.A.El-sebaii. Thermal performance of a packed bed double-pass solar air heater. Energy 32 (2007) 1524–1535.

[22] M.S. Shodha, N.K.Bansal. Analysis of a non-porous double-flow solar air heater. Applied Energy 12. (1982) 251-258.

[23] N.E. Wijeysundera, L. A. Thermal performance study of two-pass solar air heaters. Solar Energy 28, (1982) 363-370.

[24] Paisarn Naphon. Effect of porous media on the performance of the double-pass flat plate solar air heater, International Communications in Heat and Mass Transfer 32 (2005) 140 – 150.

[25] Prasad, B. a.. Effect of artificial roughness on heat transfer and friction factor in a solar air heater. Solar Energy 41, (1988).555-560.

[26] Sadık Kakaç, R. K. Handbook of single-phase convective heat transfer. New York: John Wiley and sons, (1987).

[27] Sanjay Yadav, M. K.. Nusselt number and friction factor correlations for solar air heater duct having protrusions as roughness elements on absorber plate. Experimental Thermal and Fluid Science 44, (2013) 34-41.

[28] Saini, J.S., Artificial roughness- A potential method of enhancement of efficiency of solar air heater, National conference on Emerging Energy Technologies (NCEET-2003), NIT Hamirpur.

[29] S.K. Saini, R.P. Saini. Development of correlations for Nusselt number and friction factor for solar air heater with roughened duct having arc-shaped wire as artificial roughness, Solar Energy 82 (2008) 1118–1130.

[30] Sparrow, E.M., Hossfeld, L.M., Effect of rounding of protruding edges on heat transfer and pressure drop in a duct, Int. J. Heat Mass Transfer 27 (1984), 1715-1723.

[31] Sudhanshu Dogra, N. C. . Effect of artificial roughness on heat transfer and friction factor characteristics in rectangular duct of a double pass solar air heater. IJMET 4, (2013) 289-298.

[32] Sukhatme, S. P. Solar energy principle of thermal collection and storage. Delhi: Tata McGraw-Hill, (2006).

[33] Sukhmeet Singh, S. C. Heat transfer and friction factor correlations of solar air heater ducts artificially roughened with discrete V-down ribs. Energy 36, (2011) 5053-5064.

[34] Sunil Chamoli, R. C. A review of the performance of double pass solar air heater. Renewable and Sustainable Energy Reviews 16, (2012) 481-492.

[35] Suppramaniam Satcunanathan, S. Deonarine. A two-pass solar air heater. Solar Energy, Vol. 15, (1973), 41-49.

[36] Varun, R.P.Saini, S.K. Singal. Investigation of thermal performance of solar air heater having roughness elements as a combination of inclined and transverse ribs on the absorber plate. Renewable Energy 33, (2008), 1398-1405.